Rab10 Regulates Macropinocytosis in Phagocytes

Zhiyong Liu[1], Enquan Xu[1], Hien Tran Zhao[2], Tracy Cole[2], Andrew B. West[1*]

[1] Duke Center for Neurodegeneration Research, Department of Pharmacology and Cancer Biology, Duke University, Durham, North Carolina, USA
[2] Ionis Pharmaceuticals Inc., Carlsbad, CA

*C.A. Information: Andrew.West@Duke.edu, 3 Genome Court, Durham, North Carolina, 27710 USA

ABSTRACT

Bulk fluid uptake and immune surveillance in phagocytes relies on a specialized form of endocytosis known as macropinocytosis. Herein, we find that GTP-bound Rab10 is recruited early to PI(3,4,5)P3-positive membrane ruffles in macrophages to facilitate macropinosome formation, early trafficking, and fast-recycling. Suppression of Rab10 in mouse and human primary monocyte-derived macrophages, dendritic cells, and microglia-like cells potently inhibits macropinocytosis without affecting phagocytosis or clathrin-mediated endocytosis. LRRK2-mediated phosphorylation of the switch II domain in Rab10 competes with EHBP1L1-binding to block macropinosome recycling tubules. With turn-over stalled, pRab10 macropinsomes mature to LAMP1-postive vesicles loaded with CCR5 (CD195). Inhibition of pRab10 with LRRK2 kinase inhibitors, or reduction of Rab10 expression, blocks AKT-activation in response to CCL5 (RANTES) exposure. These results suggest that Rab10 is a primary effector molecule of macropinocytosis, with LRRK2-mediated phosphorylation of Rab10 promoting macropinosome maturation and signaling.

INTRODUCTION

Macropinocytosis, a process originally discovered in macrophages isolated from rats [1], is a clathrin-independent form of endocytosis with many similarities to the better understood process of phagocytosis [2]. Both phagocytosis and macropinocytosis are actin-dependent, with phagocytosis mediating internalization of large and insoluble cargo and macropinocytosis supporting internalization of small and soluble particles. Constitutive macropinocytosis occurs in monocytes, macrophages, and other phagocytic cells, and may be critical for immune surveillance [2], although specific signaling pathways regulated by macropinocytosis are not well understood. Macropinocytosis can occur in non-phagocytic cells as well, usually in acute response to growth factors. Possible roles include the uptake and turn-over of misfolded proteins in Parkinson's disease (PD), Alzheimer's disease (AD), and amyotrophic lateral sclerosis (ALS) [3-5]. Without knowledge of proteins that specifically regulate macropinocytosis in endocytosis, most studies have explored the process using small molecule inhibitors EIPA (5-(N-Ethyl-N-isopropyl)amiloride) and rottlerin [6, 7]. However, while both molecules efficiently block macropinocytosis, they also affect other forms of endocytosis [2].

Rab small GTPases can selectively control endocytic processes, vesicle formation, trafficking and maturation, and recycling and degradation [8, 9]. In phagocytosis, Rab35 drives phagosome formation, whereas Rab20 is critical in phagosome maturation [10]. Rab proteins specific for macropinocytosis, macropinosome formation, and macropinosome maturation, have not previously been identified. The *Rab10* gene is linked to human disease in several ways. Genetic variants in *Rab10* associate with resilience to AD, and a phosphorylation site in the Rab10 switch II domain is upregulated by PD-associated mutations in the LRRK2 protein kinase [11]. LRRK2-mediated phosphorylation of Rab10 is strongly affected by all known pathogenic mutations as well as PD-risk factor genetic variants like G2385R, with Rab10 phosphorylation changing the affinity of different binding proteins to the Rab10 effector loops [12]. Our past work, consistent with others, suggests LRRK2 phosphorylation of Rab10 may prolong Rab10 in a GTP-bound state by inhibiting Rab10 interactions with GAP proteins [13]. While the specific role of Rab10 in cells linked to neurodegeneration is under investigation, recent work demonstrates Rab10 downregulates ciliogenesis in some types of cells and neurons in the brain [14]. Further, in Cos-7 cell lines, Rab10 may regulate ER dynamics and morphology [15]. Finally, Rab10 may facilitate the traffic of toll-like receptor (TLR) complexes from the Golgi to the plasma membrane in macrophages exposed to lipopolysaccharides (LPS) [16]. This regulation may have relevance for TLRs important in binding protein fibrils associated with neurodegenerative diseases [17].

Herein, we find Rab10 expression drives the formation and maturation of macropinosomes in primary human and mouse phagocytic cells, without affecting other types of endocytosis or TLR4 signaling. While Rab10-positive macropinosomes rapidly recycle, locking Rab10 in a GTP-bound state stalled the vesicles in the cytoplasm that matured through EEA1-positive to LAMP1-positive endosomes. LRRK2-mediated phosphorylation of Rab10 mimicked GTP-bound Rab10 through blocking EPHLP1 binding in the Rab10 effector loop. Finally, through immunostaining approaches, we found that macropinosomes are transport vesicles for the GPCR-chemokine receptor C-C chemokine receptor type 5 (CCR5). Reducing Rab10 expression, or blocking LRRK2-mediated Rab10 phosphorylation, inhibited the formation of CCR5-positive signaling endosomes and phospho-AKT levels. Together, these results provide evidence that Rab10 critically drives macropinocytosis, with the potential for mediation of different immune responses. Rab10 knockdown provides a new approach to attenuate constitutive macropinocytosis in different innate immune cells to better understand the link between Rab10 and human diseases.

RESULTS

Rab10 knockdown impairs macropinocytosis without affecting phagocytosis or clathrin-mediated endocytosis

Recent RNA sequencing and single-cell sequencing approaches have highlighted selective high expression of Rab10 in phagocytes that include monocytes and macrophages (Extended data Figure 1). The only known protein kinase to phosphorylate Rab10, LRRK2, shares a similar restricted expression profile in immune cell subtypes (Extended data Figure 1). In recent contributions to the development of validated monoclonal antibodies directed to Rab10 (validated with Rab10 knockdown, Extended data Figure 2), we could localize Rab10 to well defined patches of endogenous protein in macrophage plasma membrane ruffles. These ruffles persisted into clear (but short-lived) detached Rab10-positive vesicles in the cytoplasm (Extended data Figure 2). This process in macrophages, highlighted by Rab10, appeared structurally reminiscent of constitutive macropinocytosis inherent to phagocytic cells.

To determine if Rab10 knockdown affects endocytosis in phagocytic cells, we first optimized effective knockdown strategies in macrophages that did not activate or induce morphological changes in the cells. We found traditional RNA interference approaches we have utilized in the past [18] were low efficiency in primary monocyte-derived macrophages targeting a long-lived protein like Rab10 (i.e., lentivirus, rAAV2/1, or nucleofection) due to profound alterations of plasma membrane morphologies days after exposures. In contrast, incubations with low micromolar concentrations of 3rd generation anti-sense oligonucleotides (ASOs) efficiently reduced Rab10 expression in primary cells without macrophage activation (Table 1). Rab10-directed ASOs reduced expression to ~10% of constitutive levels after two-days post ASO-exposure without affecting the expression of proteins from the same Rab-type I family including Rab8a, Rab7, Rab5, or Rab3a (Figure 1A,B). Feeding macrophages 70 kDa fluorescent dextran, a canonical marker used to highlight macropinosomes, or IgG-beads (used to highlight phagosomes), or fluorescent transferrin, revealed a severe impairment only in dextran uptake due to Rab10 deficiency (Figure 1C-F). We applied the same Rab10 knockdown strategy to both human and mouse primary monocyte-derived cells polarized to macrophages (treated with M-CSF), dendritic cells (treated with GM-CSF), or microglia-like cells (treated with IL-34, NGF-β, CCL2), and in each case dextran-uptake was specifically inhibited. The degree of reduction was comparable to micromolar-exposures of the small molecule macropinocytosis inhibitor EIPA (Figure 1G-N). Results and effect sizes with Rab10 knockdown in impairing macropinocytosis, without affected phagocytosis, were robustly replicated in several other phagocyte cell lines and primary-cultured cells from both human and mouse, and with a second independent ASO targeting Rab10 (Extended data Figure 3).

Rab10 regulates macropinosome formation, maturation, and recycling

To pinpoint Rab10 entry into ruffled membrane, vesicle budding, and vesicle maturation, co-localization experiments with the PLCδ-PH-domain revealed initial exclusion of Rab10 from the beginning of circular cupping known to be regulated by ARF and Rac1-GTPases (Figure 2A,B) [19]. Further, only sparse Rab10 expression could be localized to dextran-loaded SARA-FYVE domain-positive vesicles, known to be regulated in part by Rab21 and Rab5-GTPases in endocytosis [20]. In contrast, nearly all Rab10-positive dextran-loaded vesicles were labeled with the AKT-PH domain, suggesting most Rab10 expression on macropinosomes is coincident with PIP_3/PI(3,4,)P_2 lipids. Accordingly, brief application of wortmannin, a phosphatidylinositol 3-kinase inhibitor, completely ablated all Rab10-positive vesicles in the cell (Figure 2C).

Our previous experiments, consistent with others [12-14], reveal that a small proportion of Rab10 protein in transfected cell lines (HEK-293, ~5-10% phosphorylated of total) is phosphorylated in the switch II loop at residue T73 through LRRK2 kinase activity. Using a monoclonal antibody directed to pT73-Rab10 (pRab10), we found a discrete subset of Rab10-positive macropinosomes in the cytoplasm was phosphorylated by LRRK2 (Figure 3). pRab10-macropinosomes loaded with dextran were often positive for early endosomal markers (i.e., Rab5) in contrast to non-pRab10-macropinosomes. Further, substantial subsets of pRab10-vesicles were positive for Rab7 or LAMP1 staining and DQ-ova fluorescence, features very rare in the total Rab10-positive macropinosome pool (Figure 3A-C). Macropinosomes are known to be short-lived vesicles with several routes to fast-recycling, typically within ten minutes [21, 22]. In transfected Raw264.7 cells, live-cell imaging experiments revealed lifetimes of total Rab10 vesicles of less than ten minutes, with a subset of macropinosomes dropping most eGFP-Rab10 expression in exchange for mRuby-Rab5 in about eight minutes (Extended data figure 4). We were unable to directly image or predict the formation of pRab10 vesicles from the total Rab10 vesicle pool in living cells due to the technical inability to visualize phosphorylation in living cells. However, bath-application of cells (~30 minutes) with the highly-selective LRRK2 kinase inhibitor, MLi2 (100 nM), completely ablated the pRab10-positive vesicle pool, and all pRab10 expression, suggesting pRab10-positive vesicles are exclusively dependent on LRRK2 kinase activity in these cells. Notably, MLi2 exposure did not influence the uptake of dextran, suggesting LRRK2-phosphorylation is unimportant in initial macropinocytosis (Extended data figure 5).

Our previous work in HEK-293 cells transfected with LRRK2 and Rab10 suggested LRRK2 phosphorylation of Rab10 may prolong Rab10 in a GTP-bound state by blocking Rab10-GAP interactions that occur near the phosphorylation site of the switch II domain [13]. Macrophage cells transfected with a GTP-locked version of Rab10 (Q68L) resulted in nearly all macropinosomes to stall out in the cytoplasm (Figure 4). These stalled vesicles shared the endosome vesicle marker profiles of pRab10-positive macropinosomes, including reactivity to LAMP1 (Figure 4D,E). As expected, GDP-locked Rab10 failed to associate with any vesicles in the cytoplasm. Together, these results are consistent with Rab10 controlling macropinosome formation, with LRRK2 interactions stimulating macropinosome maturation.

LRRK2 transiently interacts with Rab10 to stall macropinosome recycling

Analysis of LRRK2 subcellular localization in macrophages shows a diffuse distribution through the cytoplasm, unaffected by LRRK2 kinase inhibition, with endogenous LRRK2 protein forming transient patches of protein adjacent to pRab10-positive vesicles (Supporting data figure 2 and Figure 5A). Biochemical fractionation experiments revealed pRab10 protein primarily localized to triton-solubilized fractions, with LRRK2 binding to Rab10 independent of LRRK2 kinase activity (Figure 5B,C). Although pRab10 levels in these cells are exquisitely dependent on LRRK2 kinase activity, phos-tag analysis to resolve the stoichiometry of pRab10 from total Rab10 revealed pRab10 protein poorly interacts with LRRK2 compared to non-pRab10 in the same triton-solubilized fraction (Figure 5,C-E). These results suggest a transient interaction between non-pLRRK2 and non-pRab10 at vesicles that is destabilized by LRRK2-kinase activity.

Our efforts to directly immunoprecipitate pRab10 vesicles with pRab10 antibodies failed, possibly due to the phosphorylation site on Rab10 tightly bound to effector proteins. To help identify bound protein co-factors that may be responsible for blocking pRab10-vesicle recycling, we used a proteomics approach with GTP (vesicle-bound) or GDP (cytosolic)-swapped immunoprecipitated Rab10 protein combined with lysates from

macrophages and antibodies to total-Rab10. This approach capitalizes on the evidence that LRRK2-mediated pRab10 partially mimics a stabilized GTP-bound Rab10. We identified only one Rab10 protein interactor exclusive to GTP-bound Rab10 that was not present with GDP-bound Rab10, EH domain-binding protein 1-like protein 1 (EHBP1L1, Extended data Figure 6). Pull-down analysis with triton-solubilized and immobilized pRab10 and non-pRab10-beads demonstrated pRab10 weakly interacted with EHBP1L1 compared to non-pRab10 (Figure 6A,B). EHBP1L1 interacts with GTP bound Rab10 to regulate the formation of tubular recycling endosomes in Hela cells [23, 24]. In Raw264.7 cells transfected with eGFP(N-term)-Rab10 and Myc-mRFP(N-term)-EHBP1L1, Myc-mRFP(N-term)-EHBP1L1 prominently colocalized with Rab10 on recycling tubules. RILPL2, which was shown to be a pRab10 specific adaptor [14], localized exclusively on the body of the Rab10 positive macropinosomes and never on recycling tubules (Figure 6C,D). pRab10-vesicles, enriched with RILPL2 (Extended data figure 7), failed to form recycling tubules that are characteristic of short-lived macropinsomes (Figure 6E,F), consistent with pRab10 demarcating macropinosomes that are stalled in the cytoplasm. Over-expression of EHBP1L1 blocked LRRK2-phosphorylation of Rab10, mimicking the effects of LRRK2 kinase inhibition (Figure 6G,H). These results favor a model whereby LRRK2 kinase activity and Rab10-phosphorylation competes with EHBP1L1-binding in mediation of macropinosome fast-recycling or maturation to EEA1-positive and finally LAMP1-positive vesicles.

Rab10 and LRRK2 potentiate CCL5-stimulated AKT-signaling

Rab10 has been previously shown to regulate TLR4 trafficking and affect LPS-stimulated pro-inflammatory cascades [16]. However, in primary mouse bone-marrow derived macrophages, neither Rab10 knockdown nor LRRK2 inhibitor treatment (100 nM MLi2) altered LPS-stimulated TLR4-Myd88-dependent phosphorylation of p38 or phosphorylation of AKT (Extended data figure 8). Recent work suggests some intergrins and G protein-coupled receptors (GPCRs) can be internalized through macropinocytosis in myeloid cells like macrophages [25, 26]. Notably, HIV-1 (i.e., gp120) anchors onto CCR5 for internalization into macrophages via macropinocytosis [27]. Subcellular localization of CD11b and CCR5 in mouse bone-marrow derived macrophages revealed nearly all Rab10 and pRab10 vesicles were loaded with CCR5 (Figure 7A,B). Recent studies suggest that mature macropinosomes, enriched with $PI(3,4,5)P_3$, can also serve as efficient signaling platforms for GPCR-induced AKT phosphorylation and subsequent signal transduction [28]. Consistent with those studies, reduction of Rab10 expression, or treatment with the LRRK2 kinase inhibitor MLi2 to block pRab10 macropinosome maturation, both potently decreased CCL5-induction of AKT phosphorylation (Figure 7C-E). These results suggest that macropinocytosis may be a non-canonical but important pathway used by the GPCR CCR5 to mediate AKT phosphorylation in a rapid response to chemokines.

DISCUSSION

Phagocytic cells (e.g., macrophages) constantly survey extracellular fluid largely through macropinocytosis. Early studies demonstrated ~30% of cell volume can be internalized every hour by these macrophages, with the majority of fluid returned to the extracellular space within ten minutes [29-31]. Mechanistic insights into macropinocytosis, a process difficult to discern from phagocytosis in practice, have been largely provided through studies of viral-entry into host cells and small molecule inhibitors [6]. Using newly developed monoclonal antibodies to Rab10 together with live-cell imaging approaches, we initially observed Rab10 localization characteristics and dynamics that suggested possible function in macropinocytosis.

In the construction of a new model for macropinocytosis in phagocytic cells identified in this study (see Figure 8), Rab10 is recruited in formation prior to full plasma-membrane budding. Knockdown of Rab10 in a variety of phagocytic cells with constitutive macropinocytosis including human and mouse primary cells with macrophage, dendritic, or microglia-like polarizations resulted in profound impaired macropinocytosis without perturbation of phagocytosis or clathrin-dependent endocytosis of transferrin. Early macropinosomes distinct from the plasma membrane were Rab10 positive but lacked EEA1, with Rab10 interacting with EHBP1L1 in Rab10-positive tubules known to drive fast-recycling. Our data suggest that LRRK2-directed phosphorylation of the EHBP1L1 binding site (switch II effector loop) competes with EHBP1L1 binding, and consistent with recent reports, results in Rab10-binding to RILPL2 in vesicles.

A wealth of literature supports enrichment of CCR5 in macropinosomes that can bind HIV-1 virus for entry [27, 32]. Consistent in our cultures, all Rab10-positive macropinosomes were also loaded with CCR5. We hypothesized that stalled macropinosomes in the cytoplasm caused by LRRK2 phosphorylation may provide an important signal transduction platform for chemokines and cytokines. CCR5 is considered a critical receptor for CCL5 (RANTES) in chemotactic responses for monocytes and T cells [33, 34]. While T-cells lack substantial Rab10 expression, knockdown of either total Rab10 protein or pRab10 protein in macrophages blocked phospho-AKT induction with CCL5 exposure. We propose that macropinocytosis critically complements traditional clathrin-mediated endocytosis of some GPCRs in responding to chemokines in the extracellular space through amplification of signal transduction cascades. Our initial experiments evaluating other GPCRs like CCR2 have so-far yielded ambiguous localization to macropinosomes, suggesting specificity in the pathway that requires further study. Our results may begin to clarify how macropinocytosis associated with phagocytes in the immune system use constitutive bulk-fluid uptake for surveillance and initial response to chemokines.

Both Rab10 and the protein kinase that phosphorylates Rab10, LRRK2, demonstrate selective high expression in professional phagocytic cells. In other cell types, LRRK2 phosphorylates Rab8a in mediating ciliogenesis, with Rab10 opposing this function [35]. However, macrophages and other leukocytes are not ciliated, consistent with refined cell-type specific functions for different Rab proteins in different cells. Our previous studies in primary macrophages from mice suggest that LRRK2 kinase activity influences chemotaxis phenotypes of phagocytes in different tissues responding to a variety of immunological stimulants that include thioglycollate-induced peritonitis in the gut, over-expression of α-synuclein via rAAV2 viral transduction in the brain, or intracranial injection of LPS [36-38]. Our results here suggest that a possible mechanism underlying these observations may involve trafficking of chemokine receptors, particularly CCR5 known to be important in some of these responses. Our results suggest LRRK2 kinase activity may serve to stabilize a fraction of macropinosome-originating signaling endosomes to bolster chemokine-

receptor signaling and thus amplify the effects of chemokines like CCL5 in activating and mobilizing immune cells responding to stimuli. With both Rab10 and LRRK2 genetically linked to proteinopathies that include AD and PD, respectively, and clear roles for phagocytic immune cells in the uptake and clearance of misfolded proteins, we further speculate that the pathway discovered here may explain in part how LRRK2 and Rab10 contribute to neurodegeneration in immune cells.

METHODS

Plasmids and constructs

pCDNA3.1-GFP-Rab10 and pCDNA3.1-Flag-Rab10 were generated by insertion of synthesized Rab10 cDNA into pCDNA3.1+N-EGFP plasmid or pCDNA3.1+/N-DYK plasmid from Genscript as described (29177506). mRuby-Rab5 is kindly provided by Dr. Laura Volpicelli-Daley from University of Alabama at Birmingham. GFP-Fyve is generated by insertion of synthesized SARA1 Fyve domain into pCDNA3.1+N-EGFP plasmid from Genscript as described [39]. GFP-AKT-PH (plasmid# 21218) and GFP-PLC δ –PH (plasmid # 51407) plasmids are acquired from Addgene. pCDNA3.1-Flag-LRRK2$_{R1441C}$ is generated as previously described[40]. pCDNA3.1- RILPL2-Flag is purchase from Genscript(OHu17095). pCDNA3.1-Myc-mKate2-EHBP1L1 is generated by insertion of synthesized mKate2 and EHBP1L1(OMu05300C, Genscript) into pcDNA3.1+N-MYC plasmid from Genscript.

Cell Culture

Mouse bone marrow derived macrophages are generated by culturing the mouse bone marrow cells collected from 3-5 months old mouse in 10% Fetal bovine serum and DMEM supplemented with 20 ng/ml M-CSF. Mouse bone marrow derived dendritic cells are generated by culturing the mouse bone marrow cells in 10% Fetal bovine serum and DMEM supplemented with 20 ng/ml GM-CSF. Mouse primary microglia is collected from new born mouse and cultured as previously described [41].

Human Monocyte were acquired from frozen PBMCs with STEMCELL EasySep Human Monocyte Enrichment kit (STEMCELL TECHNOLOGIES). Purified monocytes were cultured in RPMI-1640 Glutamax medium (Invitrogen) supplemented with 10% fetal bovine serum (FBS; Atlanta Biological) , penicillin/streptomycin (Lonza) and Fungizone (2.5 ug/ml; Life Technologies). GM-CSF (all cytokines come from Peprotech, 10 ng/ml) or M-CSF (20 ng/ml) were supplemented into the monocyte culture at day 5 to induce dendritic-like cells and macrophage-like cells respectively. MDMi cells were induced as previous protocol described [42], briefly, monocytes were cultured in serum free RPMI-1640 Glutamax medium (Invitrogen) for 10 days before supplemented with GM-CSF 10 ng/ml, M-CSF 10 ng/ml, NFG-β 10 ng/ml, CCL2 100ng/ml, and IL-34 100 ng/ml.

Raw 264.7 cells (TIB-71, ATCC) were cultured in 10% Fetal bovine serum and DMEM. Raw 264.7 cells are collected at 60% confluency for transfection. Transfection was performed using Neon® Transfection System (Thermo Fisher Scientific) following the manufactory's protocol. The cells are either collected for immunoblots or fixed for microscopy 12 hours after transfection.

ASO synthesis, screening and lead identification

Synthesis and purification of all chemically purified ASOs were performed as previously described (Seth et al., J Org. Chem 2010). Approximately 500 ASOs were designed against the full mouse *Rab10* gene. ASOs were screened in days in vitro 7 (DIV7) primary mixed cortical neurons derived from embryonic day 16 C67BL/6N mice at 7 μM. ASOs were applied to culture medium for 24h, after which cells were harvested for RNA extraction and mouse *Rab10* mRNA was quantified by RT-PCR using the forward primer, reverse

primer, and probe . *Rab10* ASO 1 and 2 (Table 1) were identified among the dose-responsive ASOs in the follow-up dose-response confirmation treatment.

Immunoblotting

Protein lysates were analyzed using SDS-PAGE followed by transfer to PVDF membranes for immunoblotting with indicated primary antibodies and HRP-conjugated secondary antibodies. Signals developed with Classico ECL reagent (Millipore) was digitally detected using Chemidoc Touch (BioRad). Intensities of the indicated bands are calculated with ImageLab software. The following antibodies were used: N241A/34 anti-LRRK2 (Antibodies Inc), phospho-T73-Rab10(MJF-R21), anti-eGFP antibody (ab6673, Abcam), total Rab10 antibody (Cell signaling), anti-FLAG M2 (Sigma), anti-Myc antibody (ab32 Abcam), p38 antibody (8690, cell signaling), phospho-p38 antibody (4511, cell signaling), IRF3 antibody(4302, cell signaling), phospho-IRF3 antibody(4947 cell signaling), total AKT antibody(4691), phospho-AKT antibody(4060), β-actin (sc-47778 HRP, Santa Cruz).

Immunoprecipitation

Raw264.7 cells transfected with pCDNA3.1-Flag-Rab10 are lysed with lysis buffer containing 150 mM NaCl, 50 mM Tris-HCl, pH 7.4, 10mM $MgCl_2$, 0.05% Triton-100, 1x PhosSTOP and Protease inhibitor cocktails (Roche) followed by ultracentrifugation at 150, 000 x g for 20 min. The supernatant was collected and mixed with anti-Flag resin (M8823, sigma) for 12 hours in 4C. The beads are washed 5 times with lysis buffer and eluted with lysis buffer supplemented with 100µg/ml 3X FLAG® Peptide (F4799, sigma). The eluted lysates are analyzed using SDS-PAGE or mass spectrometer.

Mass spectrometry

Samples were reduced with 10 mM dithiolthreitol for 30 min at 80C and alkylated with 20 mM iodoacetamide for 30 min at room temperature. Next, they were supplemented with a final concentration of 1.2% phosphoric acid and 1084 µL of S-Trap (Protifi) binding buffer (90% MeOH/100mM TEAB). Proteins were trapped on the S-Trap, digested using 20 ng/µl sequencing grade trypsin (Promega) for 1 hr at 47C, and eluted using 50 mM TEAB, followed by 0.2% FA, and lastly using 50% ACN/0.2% FA. All samples were then lyophilized to dryness and resuspended in 12 µL 1%TFA/2% acetonitrile containing 12.5 fmol/µL yeast alcohol dehydrogenase (ADH_YEAST).

Quantitative LC/MS/MS was performed on 4 µL of each sample, using a nanoAcquity UPLC system (Waters Corp) coupled to a Thermo Orbitrap Fusion Lumos high resolution accurate mass tandem mass spectrometer (Thermo) via a nanoelectrospray ionization source. Briefly, the sample was first trapped on a Symmetry C18 20 mm × 180 µm trapping column (5 µl/min at 99.9/0.1 v/v water/acetonitrile), after which the analytical separation was performed using a 1.8 µm Acquity HSS T3 C18 75 µm × 250 mm column (Waters Corp.) with a 90-min linear gradient of 5 to 30% acetonitrile with 0.1% formic acid at a flow rate of 400 nanoliters/minute (nL/min) with a column temperature of 55C. Data collection on the Fusion Lumos mass spectrometer was performed in a data-dependent acquisition (DDA) mode of acquisition with a r=120,000 (@ m/z 200) full MS scan from m/z 375 – 1500 with a target AGC value of 2e5 ions. MS/MS scans were acquired at Rapid scan rate (Ion Trap) with an AGC target of 5e3 ions and a max injection time of 100 ms. The total cycle time for MS and MS/MS scans was 2 sec. A 20s dynamic exclusion was employed to

increase depth of coverage. The total analysis cycle time for each sample injection was approximately 2 hours.

The MS/MS data was searched against the SwissProt M. musculus database (downloaded in Apr 2017) and an equal number of reversed-sequence “decoys” for false discovery rate determination. Mascot Distiller and Mascot Server (v 2.5, Matrix Sciences) were utilized to produce fragment ion spectra and to perform the database searches. Database search parameters included fixed modification on Cys (carbamidomethyl) and variable modifications on Meth (oxidation) and Asn and Gln (deamidation).

Phos-tag gel analysis

PRab10 co-immunoprecipitated with LRRK2 is analyzed using SDS-PAGE gel supplemented with 100 μM $MnCl_2$ and 50 μM of Phos-Tag reagent (Wako Chemicals) as previously described (29177506,16340016). Gels are transferred to PVDF membrane followed by immunostaining using anti-Flag antibody.

Endocytosis assays

Dextran uptake assay is done by mixing of 0.1mg/ml of fluorescein labeled 70kDa Dextran (D1822, invitrogen) or tetramethylrhodamine labeled 70kDa dextran (D1818, Invitrogen) with indicated cells in 48 wells for 30mins. Phagocytosis assay is done by mixing of 0.1mg/ml of mouse IgG labeled Fluoresbrite® 641 Carboxylate Microspheres (polysciences, 17797-1) with indicated cells for 30mins. Transferrin uptake assay is done by mixing of 0.1mg/ml of alexa-488 labeled transferrin (T13342, Invitrogen) with indicated cells for 30min. Macropinosome maturation assay is done by mixing of 0.1mg/ml of DQ-conjugated ovalbumin (D12053, Invitrogen) with indicated cells for indicated time points. Phagosome maturation assay is done by mixing DQ-ovalbumin conjugated Fluoresbrite® 641 Carboxylate Microspheres with indicated cells for 30mins. Cells are washed 3 times with phosphate-buffered saline fixed with 4% paraformaldehyde for 20mins before imaging.

Immuno-fluorescence staining

Cells are fixed with 4% paraformaldehyde, washed 3 time with phosphate-buffered saline(PBS), permeabilized with PBS supplemented with 0.1% saponin, blocked with 5% goat serum and immune-stained for 12 hours with primary antibodies followed by 12hours staining with secondary antibody. Horchest is used for nucleus staining. For confocal microscopy or airyscan microscopy, cell culture coverslips are mounted on glass slides with ProLong Gold antifade mountant (Thermo Fisher Scientific). The following antibodies were used: N241A/34 anti-LRRK2 (Antibodies Inc), phospho-T73-Rab10(MJF-R21-22-5), total RAB10 antibody (MJF-R23), anti-eGFP antibody (ab6673, Abcam), anti-FLAG M2 (Sigma), anti-Myc antibody (ab32 Abcam), EEA1(sc-365652, santa cruz), LAMP1(sc-19992), CD11b(14-0112-82, Thermo Fisher Scientific), TLR4 (ab22048, Abcam), CCR5(17-1951-80 Thermo Fisher Scientific).

Widefield and super-resolution microscopy

For endocytosis assays, cells in 48 wells are imaged using Keyence bz-x700 microscope with 20x objective lens. For live cell imaging, cells cultured in 35mm glass bottom plates are imaged using Keyence

microscope with 63x Oil-Immersion Objective lens in live cell imaging chamber at 37C supplied with 5% CO_2. For high-resolution imaging, cells mounted on glass slides are imaged using Zeiss 880 Airyscan Inverted Confocal microscope with 63x Oil-Immersion Objective lens. The Airyscan images are processed using Zen 3.0 software from Zeiss.

Mice

All the mice (3-5 months of age, males and females) used in this study were bred at the University of Alabama at Birmingham (UAB). All protocols used in this study were approved by UAB Animal Care and Use Committee that is fully accredited by the AAALAC. Mouse FLAG-G2019S LRRK2 BAC (B6.Cg-Tg(Lrrk2*G2019S)2Yue/J), mouse FLAG-WT LRRK2 BAC (B6.Cg-Tg(Lrrk2)6Yue/J), LRRK2 knock out (KO) mice and non-transgenic (nTg) littermate controls (C57bL/6J) including their genotyping strategies have been described elsewhere (53-55). Quantitative PCR was used to determine the copy number of the BAC transgene from these transgenic mice and only the mice with 20-30 copies of the BAC transgene (Supplemental data) were used in this study (Primers sequence info from Sid and copy number graphs from Sid).

Statistical analyses

GraphPad Prism 6 (La Jolla, CA 92037) was used to perform all the statistical analyses: 1 way-ANOVA (with Tukey's multiple comparison test), 2 way-ANOVA (with Tukey's multiple comparison test), student's t-test and Kaplan–Meier survival curve analyses). A p value of <0.05 was considered significant for comparing groups.

REFERENCES

1. Pratten, M.K. & Lloyd, J.B. Effects of temperature, metabolic inhibitors and some other factors on fluid-phase and adsorptive pinocytosis by rat peritoneal macrophages. *Biochem J* **180**, 567-571 (1979).
2. Canton, J. Macropinocytosis: New Insights Into Its Underappreciated Role in Innate Immune Cell Surveillance. *Front Immunol* **9**, 2286 (2018).
3. Holmes, B.B. *et al.* Heparan sulfate proteoglycans mediate internalization and propagation of specific proteopathic seeds. *Proc Natl Acad Sci U S A* **110**, E3138-3147 (2013).
4. Evans, L.D. *et al.* Extracellular Monomeric and Aggregated Tau Efficiently Enter Human Neurons through Overlapping but Distinct Pathways. *Cell Rep* **22**, 3612-3624 (2018).
5. Zeineddine, R. *et al.* SOD1 protein aggregates stimulate macropinocytosis in neurons to facilitate their propagation. *Mol Neurodegener* **10**, 57 (2015).
6. Sarkar, K., Kruhlak, M.J., Erlandsen, S.L. & Shaw, S. Selective inhibition by rottlerin of macropinocytosis in monocyte-derived dendritic cells. *Immunology* **116**, 513-524 (2005).
7. Koivusalo, M. *et al.* Amiloride inhibits macropinocytosis by lowering submembranous pH and preventing Rac1 and Cdc42 signaling. *J Cell Biol* **188**, 547-563 (2010).
8. Hutagalung, A.H. & Novick, P.J. Role of Rab GTPases in membrane traffic and cell physiology. *Physiol Rev* **91**, 119-149 (2011).
9. Wandinger-Ness, A. & Zerial, M. Rab proteins and the compartmentalization of the endosomal system. *Cold Spring Harb Perspect Biol* **6**, a022616 (2014).
10. Shim, J. *et al.* Rab35 mediates transport of Cdc42 and Rac1 to the plasma membrane during phagocytosis. *Mol Cell Biol* **30**, 1421-1433 (2010).
11. Ridge, P.G. *et al.* Linkage, whole genome sequence, and biological data implicate variants in RAB10 in Alzheimer's disease resilience. *Genome Med* **9**, 100 (2017).
12. Steger, M. *et al.* Phosphoproteomics reveals that Parkinson's disease kinase LRRK2 regulates a subset of Rab GTPases. *Elife* **5** (2016).
13. Liu, Z. *et al.* LRRK2 phosphorylates membrane-bound Rabs and is activated by GTP-bound Rab7L1 to promote recruitment to the trans-Golgi network. *Hum Mol Genet* **27**, 385-395 (2018).
14. Steger, M. *et al.* Systematic proteomic analysis of LRRK2-mediated Rab GTPase phosphorylation establishes a connection to ciliogenesis. *Elife* **6** (2017).
15. English, A.R. & Voeltz, G.K. Rab10 GTPase regulates ER dynamics and morphology. *Nat Cell Biol* **15**, 169-178 (2013).
16. Wang, D. *et al.* Ras-related protein Rab10 facilitates TLR4 signaling by promoting replenishment of TLR4 onto the plasma membrane. *Proc Natl Acad Sci U S A* **107**, 13806-13811 (2010).
17. Dzamko, N. *et al.* Toll-like receptor 2 is increased in neurons in Parkinson's disease brain and may contribute to alpha-synuclein pathology. *Acta Neuropathol* **133**, 303-319 (2017).
18. Moehle, M.S. *et al.* LRRK2 inhibition attenuates microglial inflammatory responses. *J Neurosci* **32**, 1602-1611 (2012).
19. Wong, K.W. & Isberg, R.R. Arf6 and phosphoinositol-4-phosphate-5-kinase activities permit bypass of the Rac1 requirement for beta1 integrin-mediated bacterial uptake. *J Exp Med* **198**, 603-614 (2003).
20. Hu, Y., Chuang, J.Z., Xu, K., McGraw, T.G. & Sung, C.H. SARA, a FYVE domain protein, affects Rab5-mediated endocytosis. *J Cell Sci* **115**, 4755-4763 (2002).
21. Buckley, C.M. *et al.* WASH drives early recycling from macropinosomes and phagosomes to maintain surface phagocytic receptors. *Proc Natl Acad Sci U S A* **113**, E5906-E5915 (2016).
22. Kerr, M.C. *et al.* Visualisation of macropinosome maturation by the recruitment of sorting nexins. *J Cell Sci* **119**, 3967-3980 (2006).
23. Nakajo, A. *et al.* EHBP1L1 coordinates Rab8 and Bin1 to regulate apical-directed transport in polarized epithelial cells. *J Cell Biol* **212**, 297-306 (2016).

24. Rai, A. *et al.* bMERB domains are bivalent Rab8 family effectors evolved by gene duplication. *Elife* **5** (2016).
25. Gu, Z., Noss, E.H., Hsu, V.W. & Brenner, M.B. Integrins traffic rapidly via circular dorsal ruffles and macropinocytosis during stimulated cell migration. *J Cell Biol* **193**, 61-70 (2011).
26. Scarselli, M. & Donaldson, J.G. Constitutive internalization of G protein-coupled receptors and G proteins via clathrin-independent endocytosis. *J Biol Chem* **284**, 3577-3585 (2009).
27. Gobeil, L.A., Lodge, R. & Tremblay, M.J. Macropinocytosis-like HIV-1 internalization in macrophages is CCR5 dependent and leads to efficient but delayed degradation in endosomal compartments. *J Virol* **87**, 735-745 (2013).
28. Erami, Z. *et al.* Rac1-stimulated macropinocytosis enhances Gbetagamma activation of PI3Kbeta. *Biochem J* **474**, 3903-3914 (2017).
29. Steinman, R.M., Brodie, S.E. & Cohn, Z.A. Membrane flow during pinocytosis. A stereologic analysis. *J Cell Biol* **68**, 665-687 (1976).
30. Steinman, R.M., Mellman, I.S., Muller, W.A. & Cohn, Z.A. Endocytosis and the recycling of plasma membrane. *J Cell Biol* **96**, 1-27 (1983).
31. Besterman, J.M. & Low, R.B. Endocytosis: a review of mechanisms and plasma membrane dynamics. *Biochem J* **210**, 1-13 (1983).
32. Marechal, V. *et al.* Human immunodeficiency virus type 1 entry into macrophages mediated by macropinocytosis. *J Virol* **75**, 11166-11177 (2001).
33. Schall, T.J., Bacon, K., Toy, K.J. & Goeddel, D.V. Selective attraction of monocytes and T lymphocytes of the memory phenotype by cytokine RANTES. *Nature* **347**, 669-671 (1990).
34. Schall, T.J., Bacon, K., Camp, R.D., Kaspari, J.W. & Goeddel, D.V. Human macrophage inflammatory protein alpha (MIP-1 alpha) and MIP-1 beta chemokines attract distinct populations of lymphocytes. *J Exp Med* **177**, 1821-1826 (1993).
35. Dhekne, H.S. *et al.* A pathway for Parkinson's Disease LRRK2 kinase to block primary cilia and Sonic hedgehog signaling in the brain. *Elife* **7** (2018).
36. Moehle, M.S. *et al.* The G2019S LRRK2 mutation increases myeloid cell chemotactic responses and enhances LRRK2 binding to actin-regulatory proteins. *Hum Mol Genet* **24**, 4250-4267 (2015).
37. Daher, J.P. *et al.* Leucine-rich Repeat Kinase 2 (LRRK2) Pharmacological Inhibition Abates alpha-Synuclein Gene-induced Neurodegeneration. *J Biol Chem* **290**, 19433-19444 (2015).
38. Daher, J.P., Volpicelli-Daley, L.A., Blackburn, J.P., Moehle, M.S. & West, A.B. Abrogation of alpha-synuclein-mediated dopaminergic neurodegeneration in LRRK2-deficient rats. *Proc Natl Acad Sci U S A* **111**, 9289-9294 (2014).
39. Hayakawa, A. *et al.* Structural basis for endosomal targeting by FYVE domains. *J Biol Chem* **279**, 5958-5966 (2004).
40. Smith, W.W. *et al.* Kinase activity of mutant LRRK2 mediates neuronal toxicity. *Nat Neurosci* **9**, 1231-1233 (2006).
41. Lian, H., Roy, E. & Zheng, H. Protocol for Primary Microglial Culture Preparation. *Bio Protoc* **6** (2016).
42. Ryan, K.J. *et al.* A human microglia-like cellular model for assessing the effects of neurodegenerative disease gene variants. *Sci Transl Med* **9** (2017).

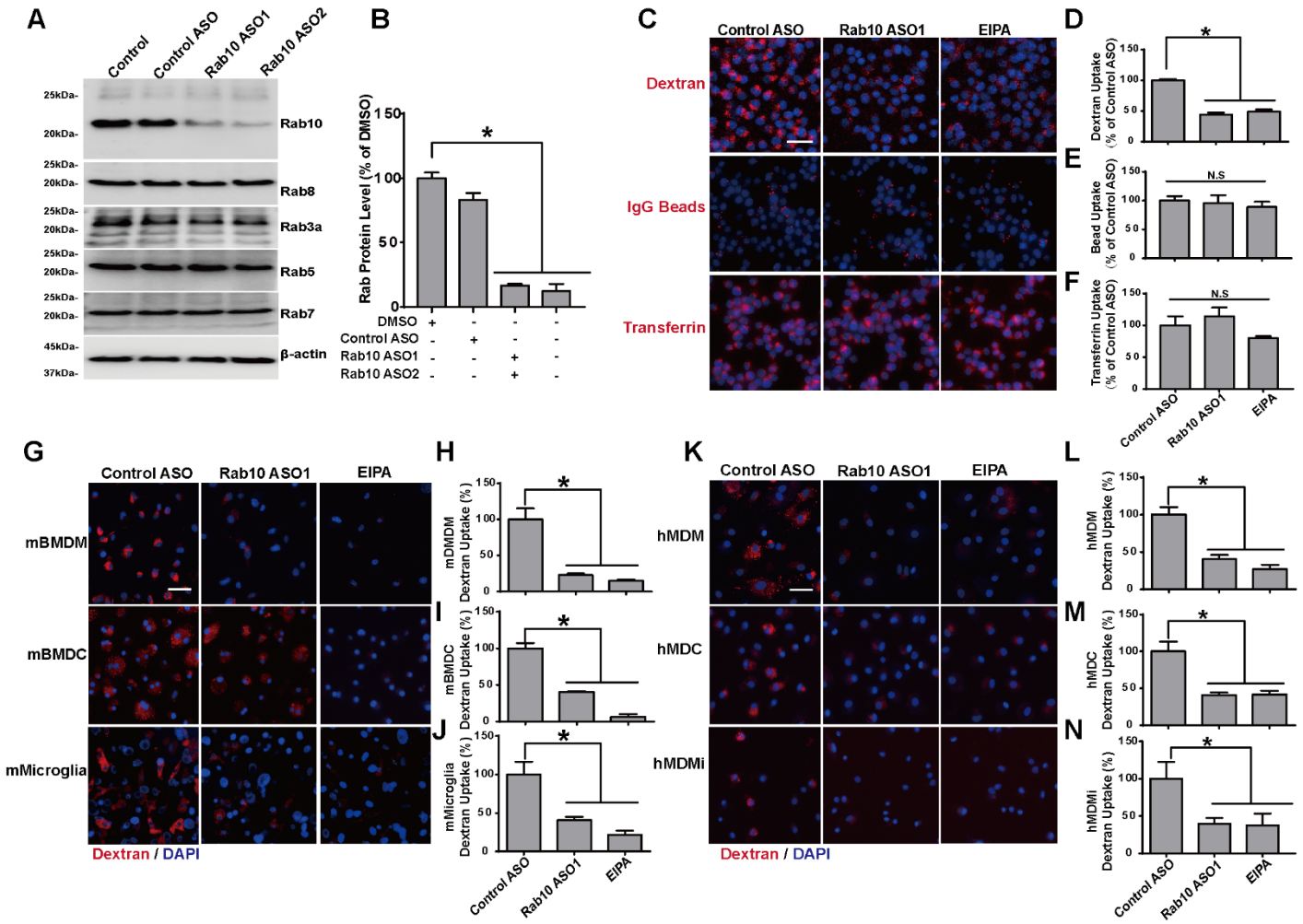

Figure 1. Rab10 expression regulates macropinocytosis.

a, Raw 264.7 macrophage cells were treated with DMSO (0.05%), 1 μM control antisense oligonucleotide (ASO), or Rab10-directed ASO (1 μM), for four days. Immunoblots are representative of three independent experiments, with similar results obtained. **b,** Calculated reduction of Rab10 (n=3 biologically independent experiments). **c,** Raw 264.7 cells were treated with the indicated ASO for four days, or 50 μM EIPA (5-[N-ethyl-N-isopropyl]amiloride) for 20 min, prior to incubation for 60 min with fluorescent (tetramethylrhodamine, TRITC)-labeled dextran (70 kDa, shown as red color), IgG-agarose, or transferrin. Representative photomicrographs (from >20 images analyzed for each conditions from n=3 biologically independent experiments) are shown from cells extensively washed, fixed and stained with DAPI (shown as blue color). **d-f,** Relative fluorescent signals (i.e., dextran uptake) were calculated as a percent of control-ASO treated cells. **g,** Primary mouse bone marrow-derived macrophage cells (BMDM) from adult male C57BL/6J mice were treated with murine cytokines directed towards a monocytic lineage (mBMDM), dendritic lineage (mBMDC), or microglia-like lineage (mMicroglia). Cells were incubated with TRITC-dextran for 30 min prior to washing, fixing, and staining with DAPI. Representative photomicrographs from >20 images analyzed for each condition from n=3 biologically independent experiments are shown. **h-j,** Relative fluorescent signals were calculated as a percent of control-ASO treated cells. **k,** Human monocytes purified from venous blood draws from healthy adult males were treated with human cytokines towards a monocytic

lineage (hMDM), dendritic lineage (hMDC), or microglia-like lineage (hMicroglia). Cells were incubated with TRITC-dextran for 30 min prior to washing, fixing, and staining with DAPI. Representative photomicrographs from >20 images analyzed for each conditions from n=3 biologically independent experiments are shown. **l-n,** Relative fluorescent signals were calculated as a percent of control-ASO treated cells. Scale bars show 50 μm. Column graphs show group means with error bars as ± SEM; significance was assessed by one-way ANOVA ($p>0.01$) with * representing Tukey's post hoc test $p<0.01$, or n.s. ($p>0.05$).

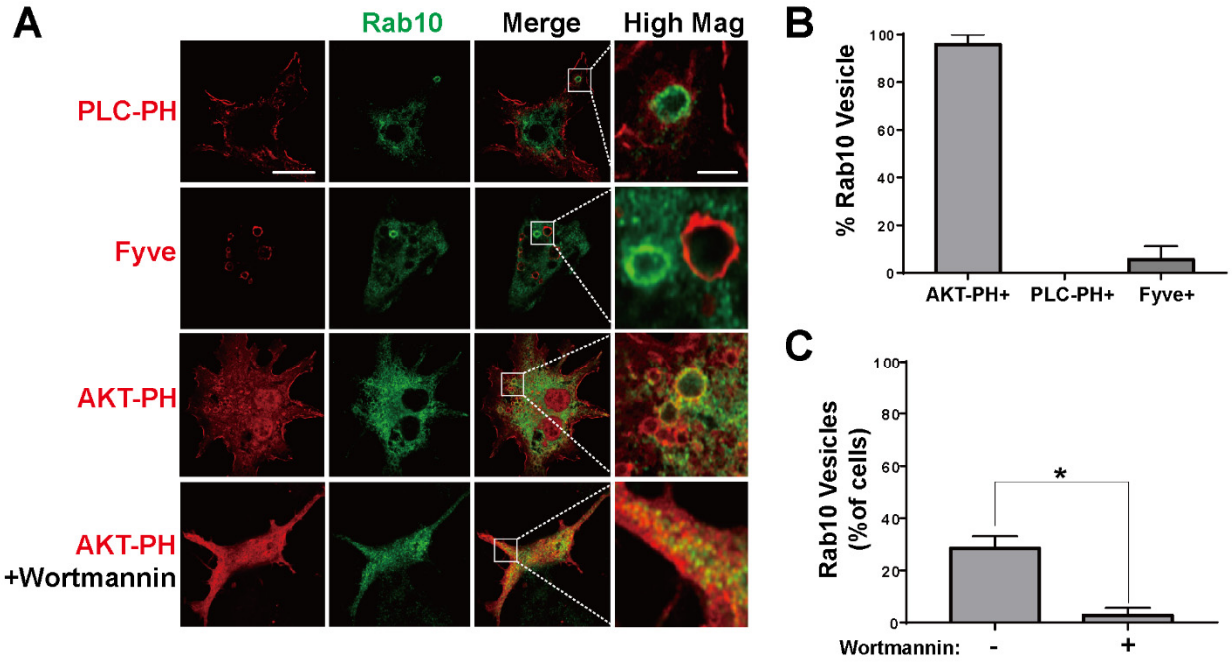

Figure 2. Rab10 binds to early plasma-membrane PIP_3/ $PI(3,4)P_2$ macropinsomes

a, Raw 264.7 macrophage cells were transfected with FLAG(N-term)-Rab10 and eGFP(C-term)-AKT-PH domain, or eGFP(C-term)-SARA-Fyve domain, or eGFP(C-term)-PLC-PH domain, and treated with or without wortmannin (1 uM) for one hour. Representative photomicrographs (from >20 images analyzed for each conditions from n=3 biologically independent experiments) are shown from fixed cells immuno-stained for Flag-tag (Rab10, shown as green) together with eGFP epifluorescence (shown as red). White bounding boxes show "High Mag" panels that magnify representative individual vesicles. Scale bars are 10 μm or 1 μm in "Hig Mag" panels. **b,** Calculated percentage of double-positive vesicles (n>50 counted from n=3 biologically independent experiments) are shown. **c,** Percent of cells in the same photomicrographs harboring Rab10 vesicles are calculated.

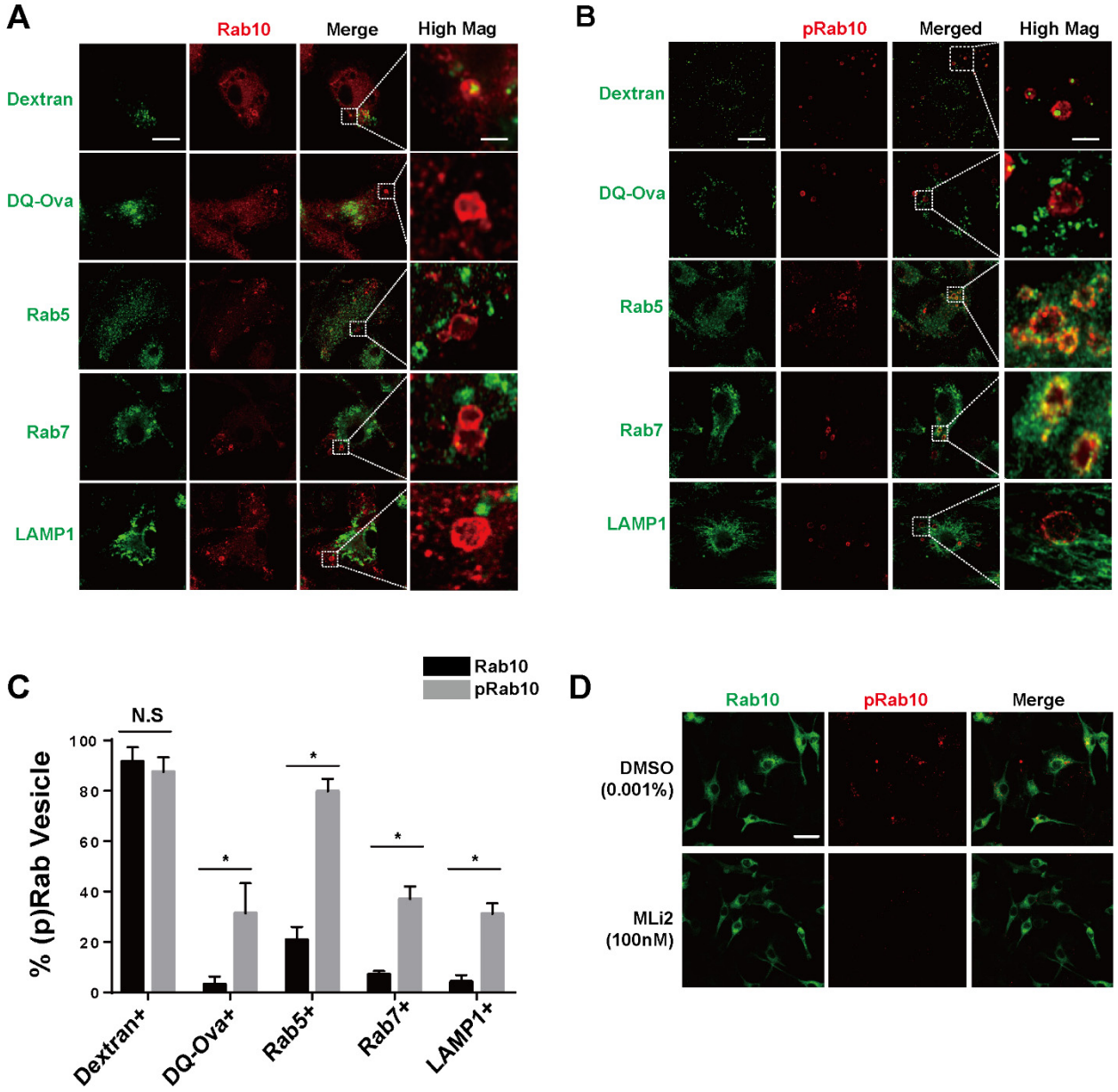

Figure 3. Phosphorylated-Rab10 vesicles mature to LAMP1-positive endosomes.

a, Primary mouse bone marrow-derived macrophage cells (BMDM) from adult male WT-LRRK2 mBAC transgenic mice were pre-incubated with FITC-conjugated dextran (70 kDa, green signal) or DQ-conjugated ovalbumin (shown as green signal) prior to washing, fixing, and immunostaining with total-Rab10 (shown as red signal), or **b,** pThr73-Rab10 antibody (shown as red signal). For Rab10-positive, dextran-loaded endosome localization, cells were also co-stained with antibodies to Rab5, Rab7 or LAMP1 (show as green signal in separate images). Representative photomicrographs (from >20 images analyzed for each condition from n=3 biologically independent experiments) are shown. Bounding boxes highlight vesicles in “High Mag” panels. Scale bars represent 10 μm and 1 μm for “High Mag” images. **c**, Calculated percentage of double-positive vesicles (n>50 counted from n=3 biologically independent experiments) are shown with error bars as ± SEM and significance was assessed by one-way ANOVA with Tukey’s post hoc test (*$p < 0.01$ for both

tests). D) Raw264.7 cells were transfected with eGFP(N-term)-WT Rab10 (show as green signal) and treated with 0.001% DMSO or 100 nM MLi2 (i.e., >IC_{90} concentration) for 2 hours prior to fixation and immunostaining with pThr73-Rab10 antibody (shown as red signal). Representative photomicrographs (from >20 images analyzed for each conditions from n=3 biologically independent experiments) are shown. Scale bars indicate 20 μm.

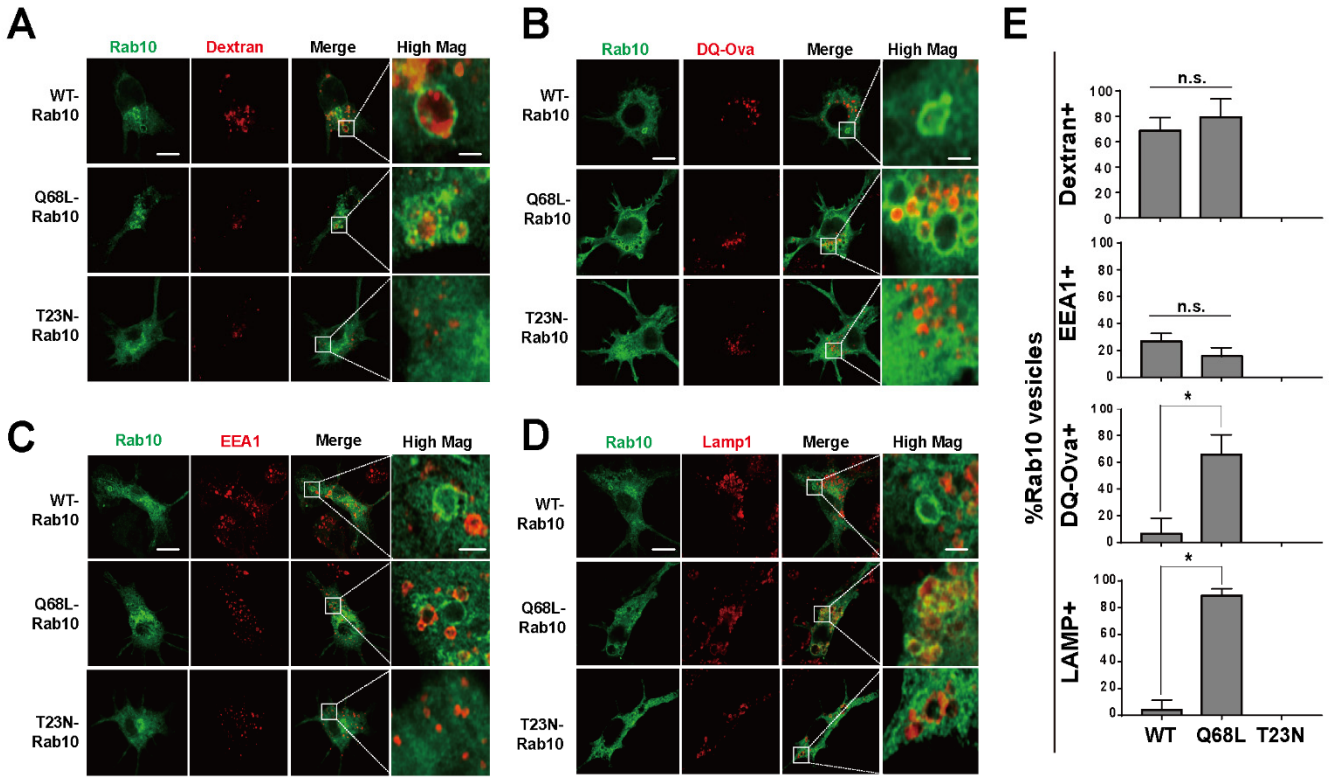

Figure 4. GTP-locked Rab10 vesicles mature to LAMP1-positive endosomes.

a, Raw264.7 cells were transfected with plasmids expressing eGFP(N-term)-WT-Rab10, Q68L-Rab10 (GTP-locked) or T23N-Rab10 (GDP-locked). 24-hours later, cells were incubated with TRITC-dextran (70 kDa, shown as red signal), or **b,** DQ-ovalbumin, for 30 min before washing and fixation. **c,** Cells were further stained for EEA1, or, **d,** LAMP1, which was detected with Cy5 dye (show as red signal). Representative photomicrographs are from >10 images analyzed for each condition from n=3 biologically independent experiments. White bounding boxes are magnified in "High Mag" panels that show individual vesicles. Scale bars represent 10 μm and 1 μm for "High Mag". **e,** Calculated percentage of double-positive vesicles (n>50 counted from n=3 biologically independent experiments) are shown with error bars as ± SEM; significance was assessed by one-way ANOVA with Tukey's post hoc test *$p < 0.01$.

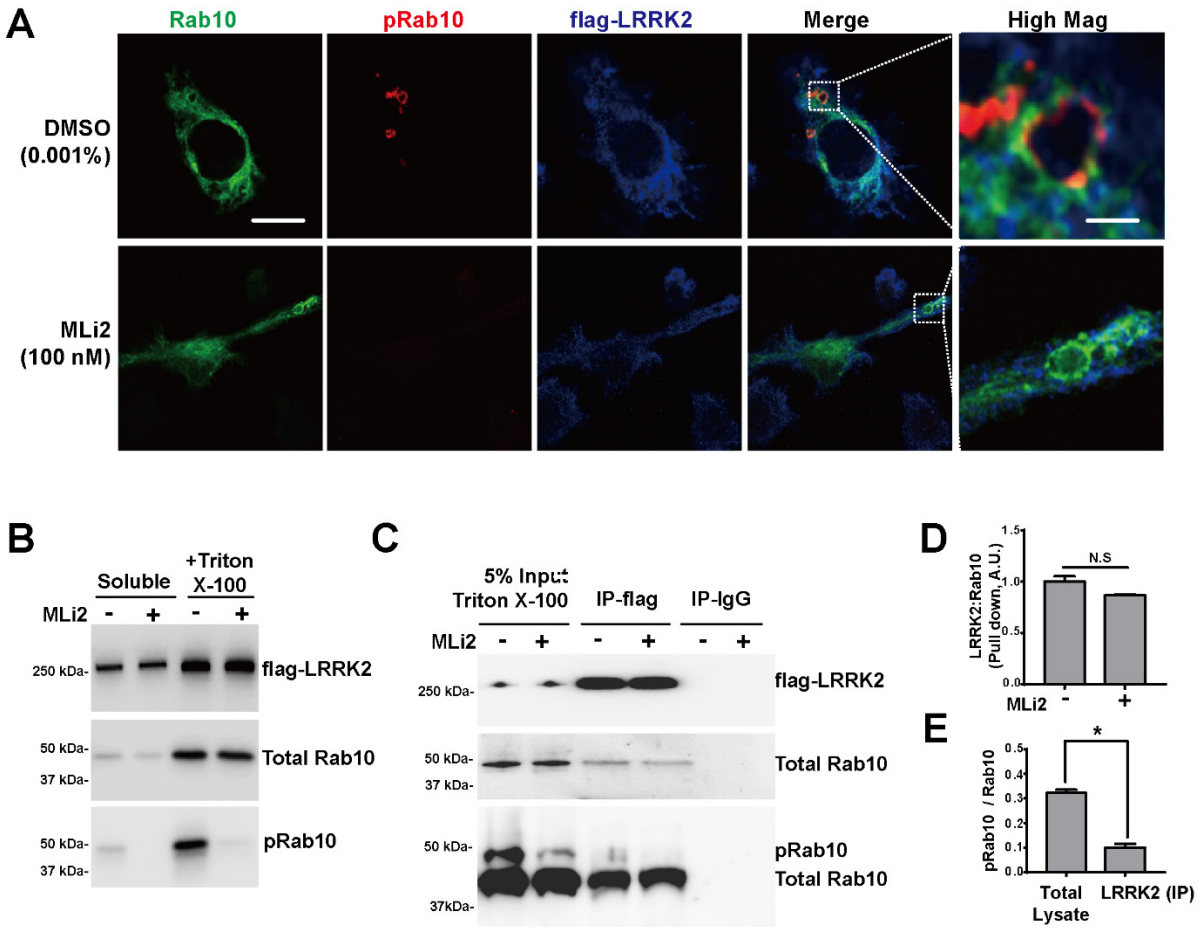

Figure 5. LRRK2 transiently interacts with Rab10-positive macropinosomes

a, Raw264.7 cells were transfected with Flag(N-term)-LRRK2 and eGFP(N-term)-Rab10 for 24 hours and treated with or without the LRRK2 kinase inhibitor MLi2 (100 nM) for 2 hours. Representative photomicrographs (from >20 images analyzed for each condition from n=3 biologically independent experiments) are shown from fixed cells with eGFP-Rab10 epifluorescence (green), and immuno-stained for pRab10 (red) and LRRK2 (blue). White bounding boxes are magnified in "High Mag" panels that show individual vesicles. Scale bars represent 10 µm or 1 µm in "Hig Mag" panels. **b,** Cells were sequentially lysed mechanically into buffer to create a 'soluble' protein fraction, pelleted, and then lysed into triton X-100 buffer. pRab10 was detected with a phospho-specific antibody. **c,** The triton X-100 lysate was used as input for LRRK2 immunoprecipitation, with subsequent detection of total Rab10 and pRab10 proteins in LRRK2:Rab10 immunocomplexes. pRab10 was detected with phos-tag gel analysis. Immunoblots are representative of three independent experiments, with similar results obtained. **d,** Calculated levels of LRRK2:Rab10 with and without LRRK2 kinase inhibition, and **e,** the ratio of pRab10 to total Rab10 protein interacting with LRRK2 in triton X-100 fractions. Data are from n=3 biologically independent experiments with error bars showing ± SEM; significance was assessed by one-way ANOVA with * representing Tukey's post hoc test $p<0.01$ or n.s. ($p>0.05$).

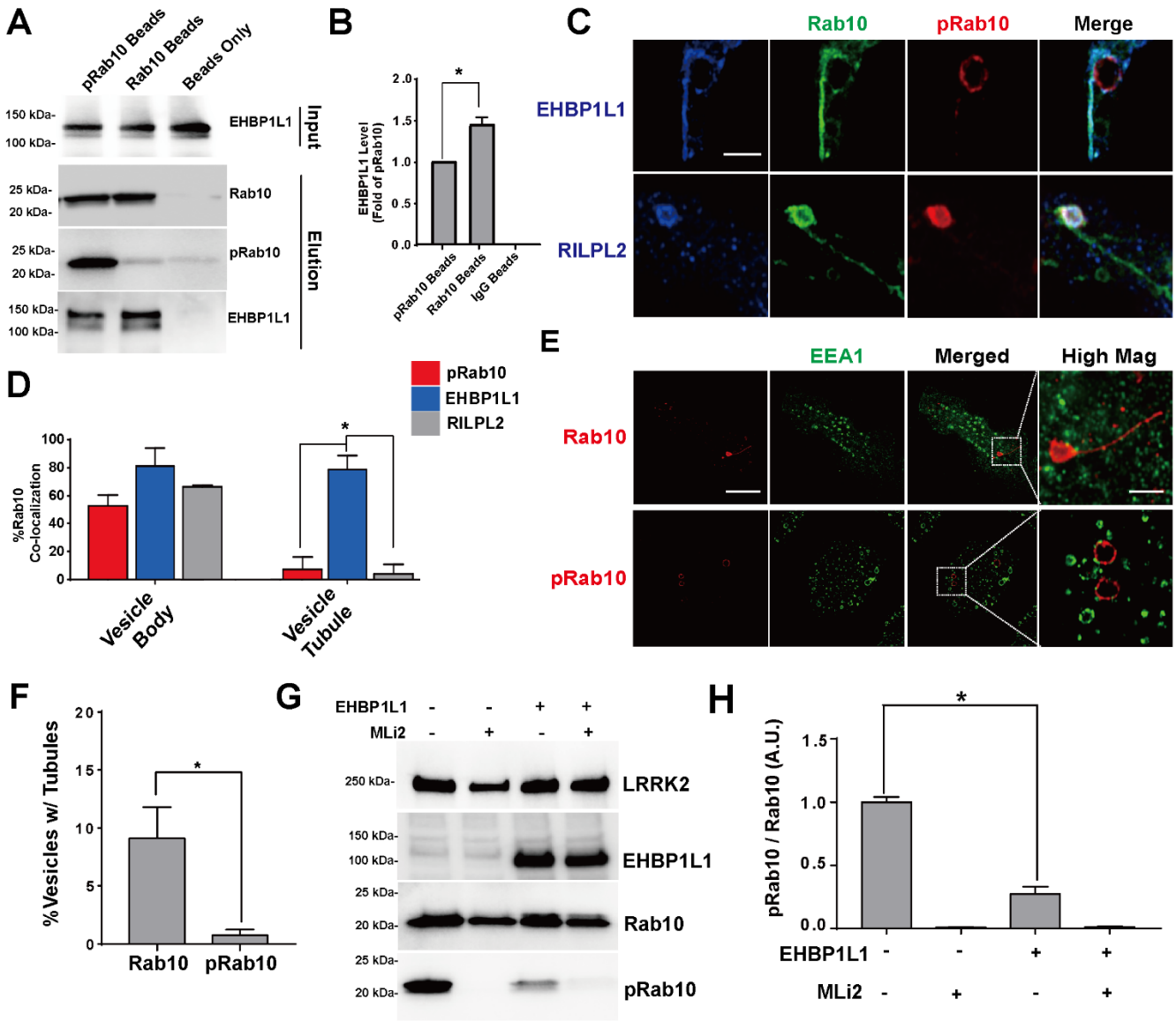

Figure 6. LRRK2 phosphorylation of Rab10 inhibits vesicle recycling by blocking EHBPL1 binding

A) HEK293 FT cells are transfected with Flag(N-term)-Rab10 and Myc(N-term)-LRRK2$_{R1441C}$ and treated with 0.001% DMSO or 100nM MLi2. Flag(N-term)-Rab10 protein is immobilized on Flag-tag resin and mixed with lysate of HEK293 cells transfected with Myc(N-term)-EHBP1L1 to form Rab10:EHBP1L1 complex. The total Rab10 and pThr73-Rab10 on the beads are detected using anti-Flag antibody and pThr73-Rab10 antibody. The EHBP1L1 in the lysates and immobilized on the beads are detected using anti-Myc tag antibody. Representative immunoblots are shown. B) The relative EHBP1L1 pulled down level is calculated as fold of EHBP1L1 pulled down with immobilized rab10 without MLi2. Data are from n=3 biologically independent experiments. C) Raw 264.7 cells are co-transfected with GFP(N-term)-Rab10 (green) and Myc(N-term)-EHBP1L1 or Flag(C-term)-RILPL2. Cells are immune-stained with anti-Myc for EHBP1L1 or anti-Flag for RILPL2(shown in blue) and anti-pThr73 for pRab10 (shown in red). Representative photomicrographs (from >20 images analyzed for each condition from n=3 biologically independent

experiments) are shown. Scale bar represents 1 μm. D) Pearson's colocalization coefficient for Rab10 and pRab10, EHBP1L1 and and RILPL2 on vesicle bodies and tubular vesicles are calculated. Data are from n=20 vesicles with tubular structures from 3 independent experiments. E) Primary mouse bone marrow-derived macrophage cells (BMDM) from adult male WT LRRK2 BAC transgenic mice are immunostained with EEA1 antibody (green) and pThr73-Rab10 antibody total Rab10 antibody (red) as indicated. Representative photomicrographs (from >20 images analyzed for each condition from n=3 biologically independent experiments) are shown. Bounding boxes are magnified in "High Mag" panels that show individual vesicles. Scale bars represent 10 μm and 1 μm for "High Mag" F) Calculated percentage of vesicles positive with tubular structures (n>50 counted from n=3 biologically independent experiments) are shown. G) Raw264.7 cells are co-transfected with Flag(N-term)-Rab10, Flag(N-term)-LRRK2$_{R1441C}$ and Myc(N-term)-EHBP1L1, representative immunoblots are shown. H) The relative pThr73-Rab10 level is calculated as fold of cells transfected with Flag(N-term)-Rab10 and Flag(N-term)-LRRK2 only. Data are from n=3 biologically independent experiments. Error bars show ± SEM; significance was assessed by one-way ANOVA with * representing Tukey's post hoc test $p<0.01$ or n.s. ($p>0.05$).

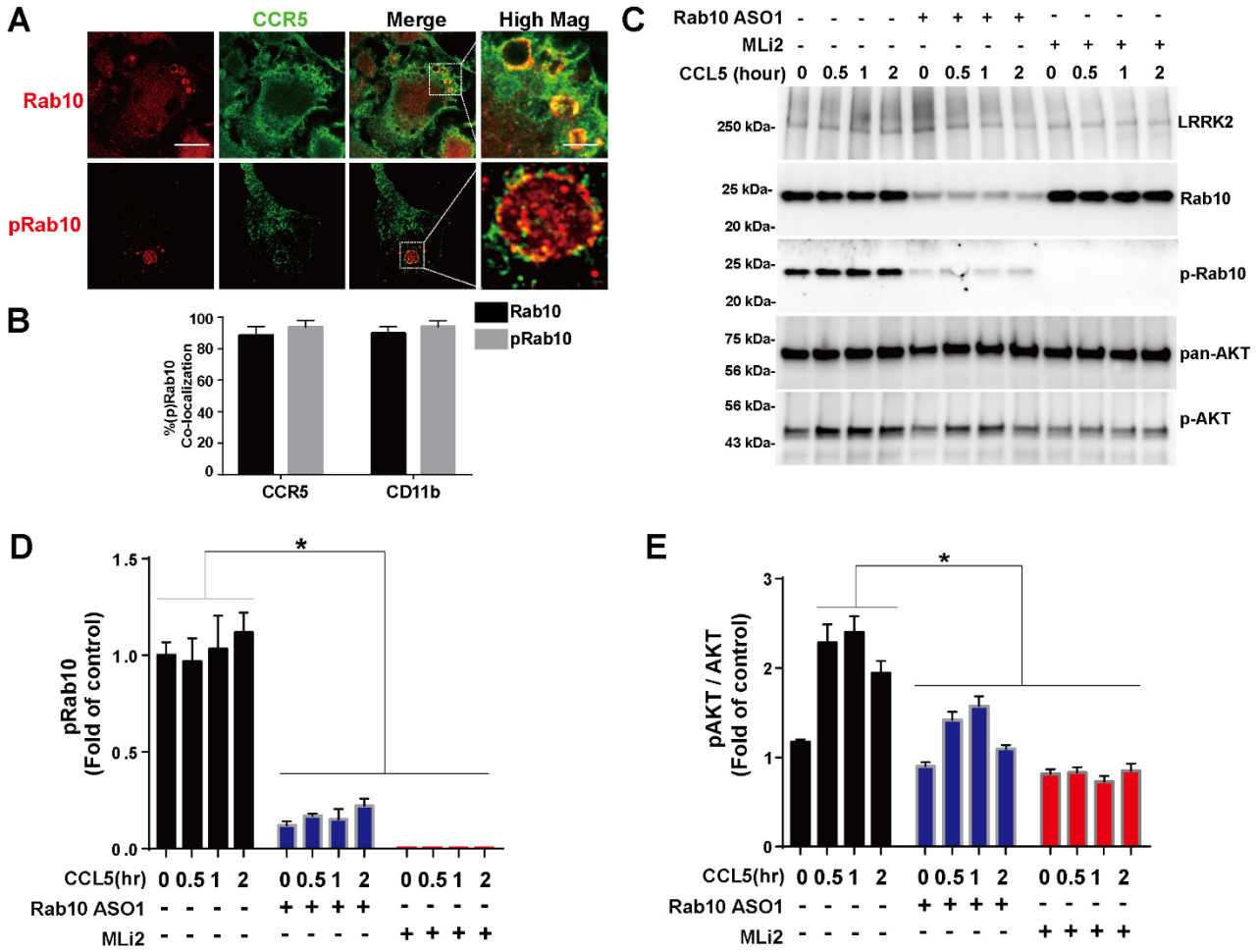

Figure 7. LRRK2 phosphorylation of Rab10 promotes CCL5-induced AKT phosphorylation

A) Primary mouse bone marrow-derived macrophage cells (BMDM) from adult male WT LRRK2 BAC transgenic mice are immunostained with anti-mouse CCR5 antibody (green) and total Rab10 antibody or pThr73 Rab10 antibody (red) as indicated. Representative photomicrographs (from >20 images analyzed for each condition from n=3 biologically independent experiments) are shown. Bounding boxes are magnified in “High Mag” panels that show individual vesicles. Scale bars represent 10 μm and 1 μm for “High Mag” B) Calculated percentage of double-positive vesicles (n>50 counted from n=3 biologically independent experiments) are shown. C) Primary mouse bone marrow-derived macrophage cells (BMDM) from adult male WT LRRK2 BAC transgenic mice are treated with DMSO, 1 μM Rab10 ASO for 4 days or 100nM MLi2 for 12 hours before stimulated with 100nM CCL5 for indicated time points. Representative immunoblots from n=3 biologically independent experiments are shown. D) Relative pRab10 level is calculated as fold of cells treated without Rab10 ASO1, CCL5 or MLi2. E) Relative pSer473-AKT level is normalized to total AKT and calculated as fold of cells treated without Rab10 ASO1, CCL5 or MLi2. Data are means ± SEM; significance is assessed by one-way ANOVA with Tukey’s post hoc test. *P < 0.01.

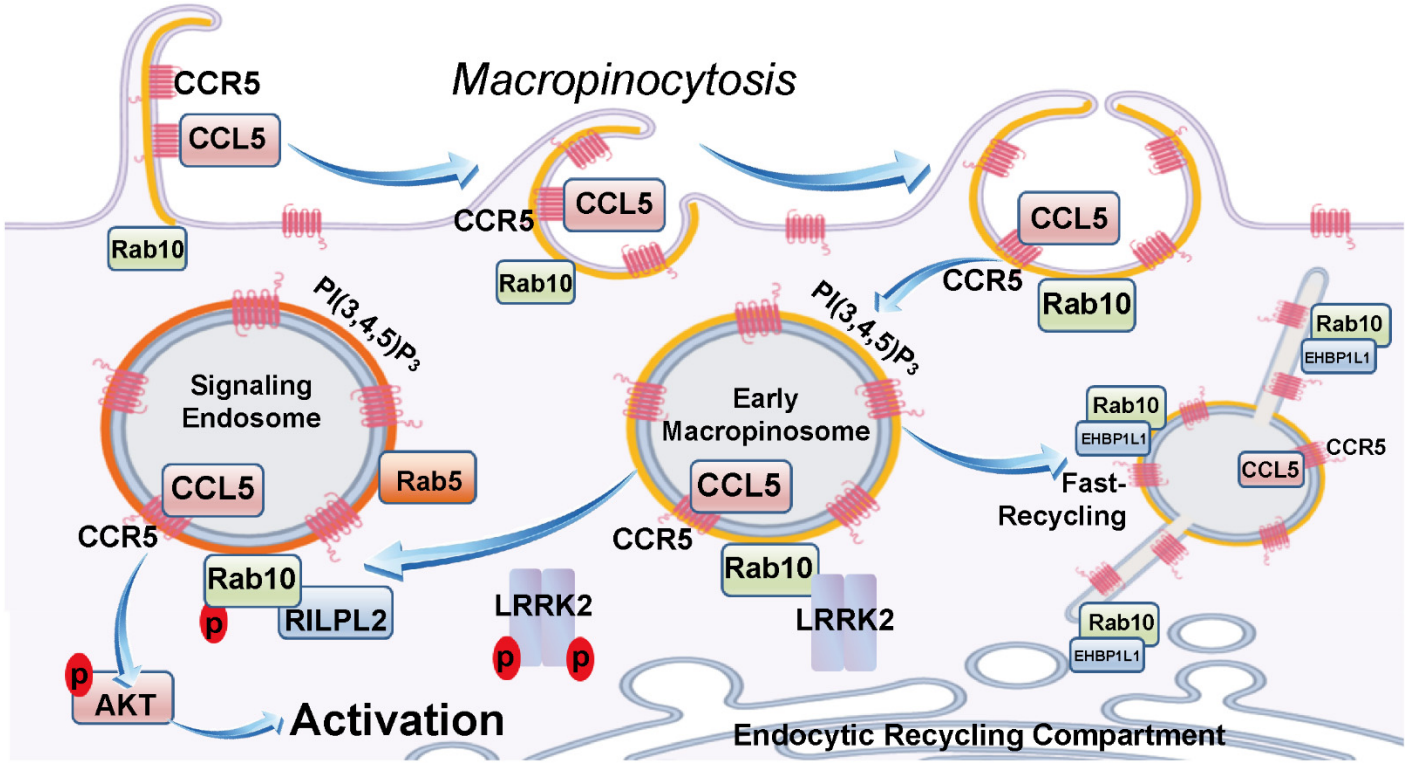

Figure 8. Model of the role of Rab10 and LRRK2 in regulation of macropinosome early maturation, recycling and signaling.

Rab10 is initially recruited to the PI(3,4,5)P_3 positive membrane ruffles at the early stage of macropinosome formation. During the process the ruffle closure, PI(3,4,5)P_3 is concentrated on macropinosomes, which recruits more Rab10 to facilitate early trafficking of macropinosomes. Without LRRK2 phosphorylation, Rab10 binds EHBP1L1 and facilitate the fast recycling of surface receptors such as CCR5. LRRK2 phosphorylation of Rab10 on Thr73 inhibits the binding of Rab10 and EHBP1L1 and enhanced the binding between RILPL2 and Rab10, therefore inhibit the fast recycling of CCR5 and retained CCR5 on macropinosomes. CCR5 retained on macropinosomes can further interact with the CCL5 internalized through macropinocytosis and activates AKT signaling pathway using PI(3,4,5)P_3 enriched macropinosomes as signaling platform.

Table 1 Sequences of antisense oligos. Black: unmodified deoxyribose (2'H); orange: 2' methoxyethyl (MOE). Unmarked linkages: phosphorothioate (PS); linkages marked with o: normal phosphodiester (PO). mC: 5-methylcytosine.

ASO	Sequence
Control ASO "Ionis 676630" (CTRL)	mCmCoToAoTAGGAmCTATmCmCAoGoGoAA
Rab10 "Ionis 978453" (ASO1)	TmComCGoAAATATGTGGTAoGoTAmC
Rab10 "Ionis 978554" (ASO2)	GToTToCAGGATATGATmCoGoGmCT

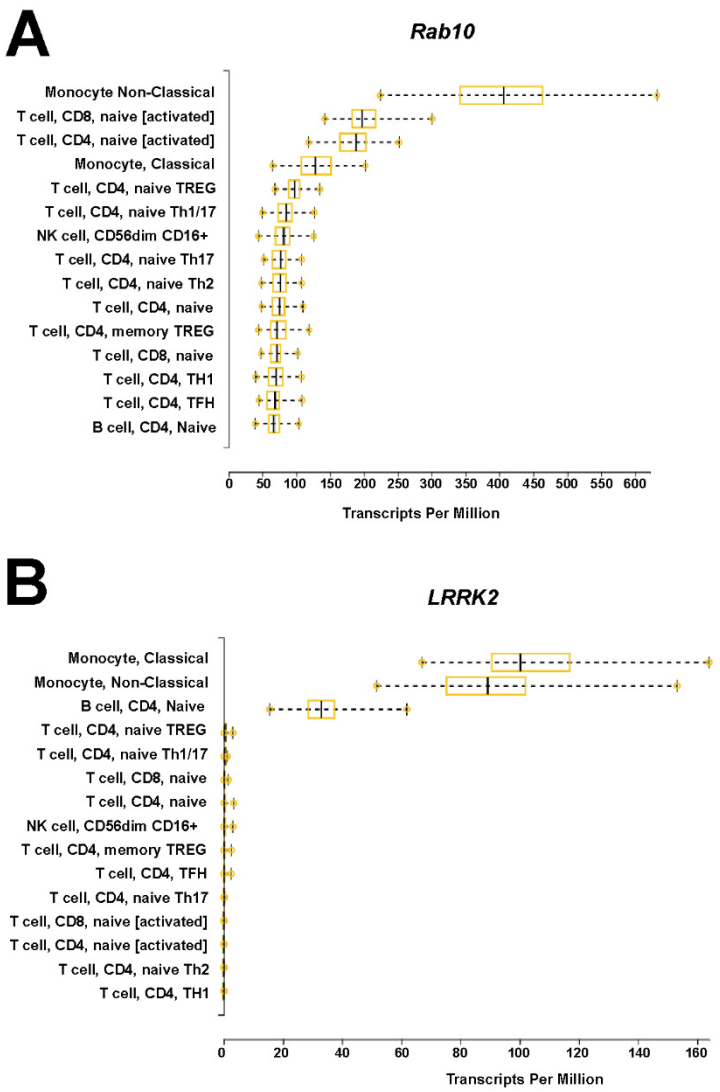

Extended data figure 1. Rab10 and LRRK2 selective co-expression in monocytes

A) Expression profiles of Rab10 and B) LRRK2 in different immune cells. Results are adapted from DICE (Database of Immune Cell Expression, Expression quantitative trait loci eQTLs, and Epigenomics, https://dice-database.org/)

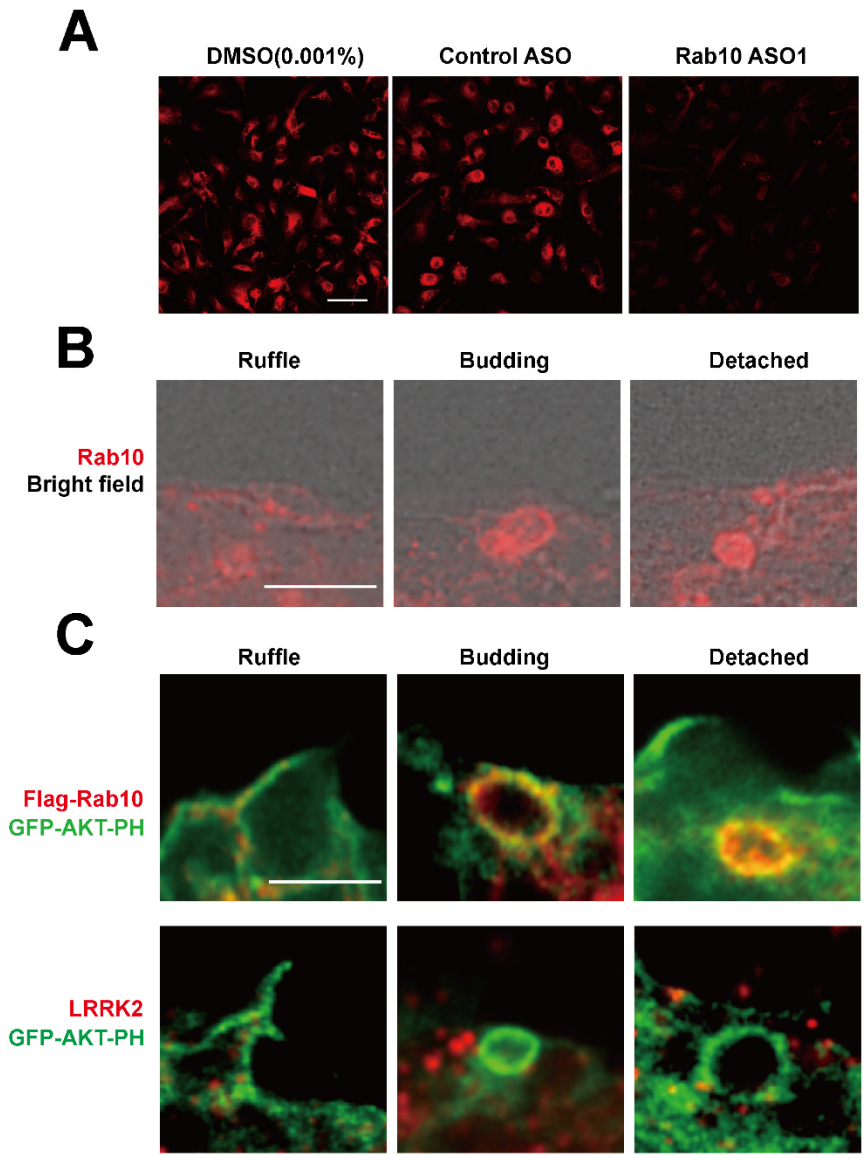

Extended data figure 2. Rab10-positive vesicles emergent from ruffled plasma membrane in macrophages

a, Mouse bone marrow derived macrophages (BMDMs) treated with DMSO, control ASO or ASO1 were fixed and immune-stained with anti-total-Rab10 antibody (shown in red). Representative confocal images are shown. Scale bar represents 50 μm. **b**, Mouse bone marrow derived macrophages (BMDMs) were fixed and immuno-stained with anti-total-Rab10 antibody (shown in red). Plasma membrane was imaged with wide-field fluorescence microscopy overlaid with phase contrast (shown in grey). Representative images are shown. Scale bar represents 2 μm **c,** Raw264.7 cells were co-transfected with Flag(N-term)-Rab10 or LRRK2, with eGFP-tagged AKT-PH domain. Cells were fixed and immuno-stained with Flag-tag antibody, LRRK2 (shown in red), with epifluorescence (shown in green). Representative photomicrographs shown. Scale bar represents 1 μm.

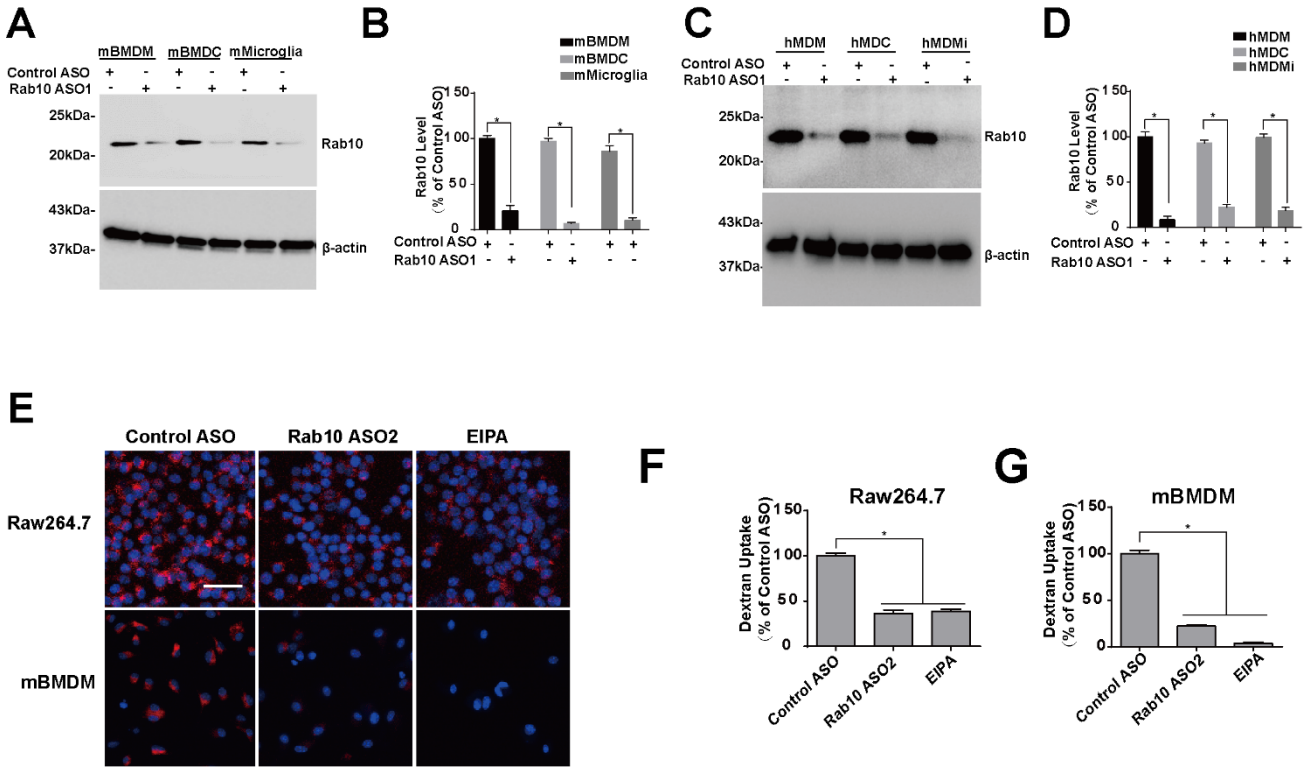

Extended data figure 3. Rab10 expression is required for macropinocytosis in human and mouse phagocytic cells

a, Primary mouse bone marrow-derived macrophage cells (BMDMs) from adult male C57BL/6J mice were differentiated to a monocytic lineage (mBMDM), dendritic lineage (mBMDC), or microglia-like lineage (mMicroglia). Cells were treated with 1 μM control ASO or Rab10 ASO1 for four days before harvesting protein lysate and immunoblotting. Representative immunoblots from three biologically independent experiments are shown. **b**, Relative Rab10 level is calculated as % of mBMDM cells treated with control ASO. **c**, Human monocytes purified from human venous blood from healthy adult males were were differentiated to a monocytic lineage (hMDM), dendritic lineage (hMDC), or microglia-like lineage (hMDMi). Cells were treated with 1 μM control ASO or Rab10 ASO1 for four days before harvesting protein lysate and immunoblotting. Representative immunoblots from three biologically independent experiments are shown. **d**, Relative Rab10 level is calculated as % of hMDM cells treated with control ASO. **e**, Raw264.7 cells and mBMDM cells derived from C57BL/6J mice were treated with control ASO or Rab10 ASO2 for 4 days, or 50 μM EIPA (5-[N-ethyl-N-isopropyl]amiloride) for 20 min, prior to incubation for 60 min with fluorescent (tetramethylrhodamine, TRITC)-labeled dextran (70 kDa, shown as red signal). Representative photomicrographs (from >20 images analyzed for each conditions from n=3 biologically independent experiments) are shown from cells extensively washed, fixed, and stained with DAPI (shown as blue signal). **f,g**, Relative fluorescent signals were calculated as a percent of control-ASO treated cells. Scale bars show 50 μm. Column graphs show group means with error bars as ± SEM; significance was assessed by one-way ANOVA with * representing Tukey's post hoc test $p<0.01$ or n.s. ($p>0.05$).

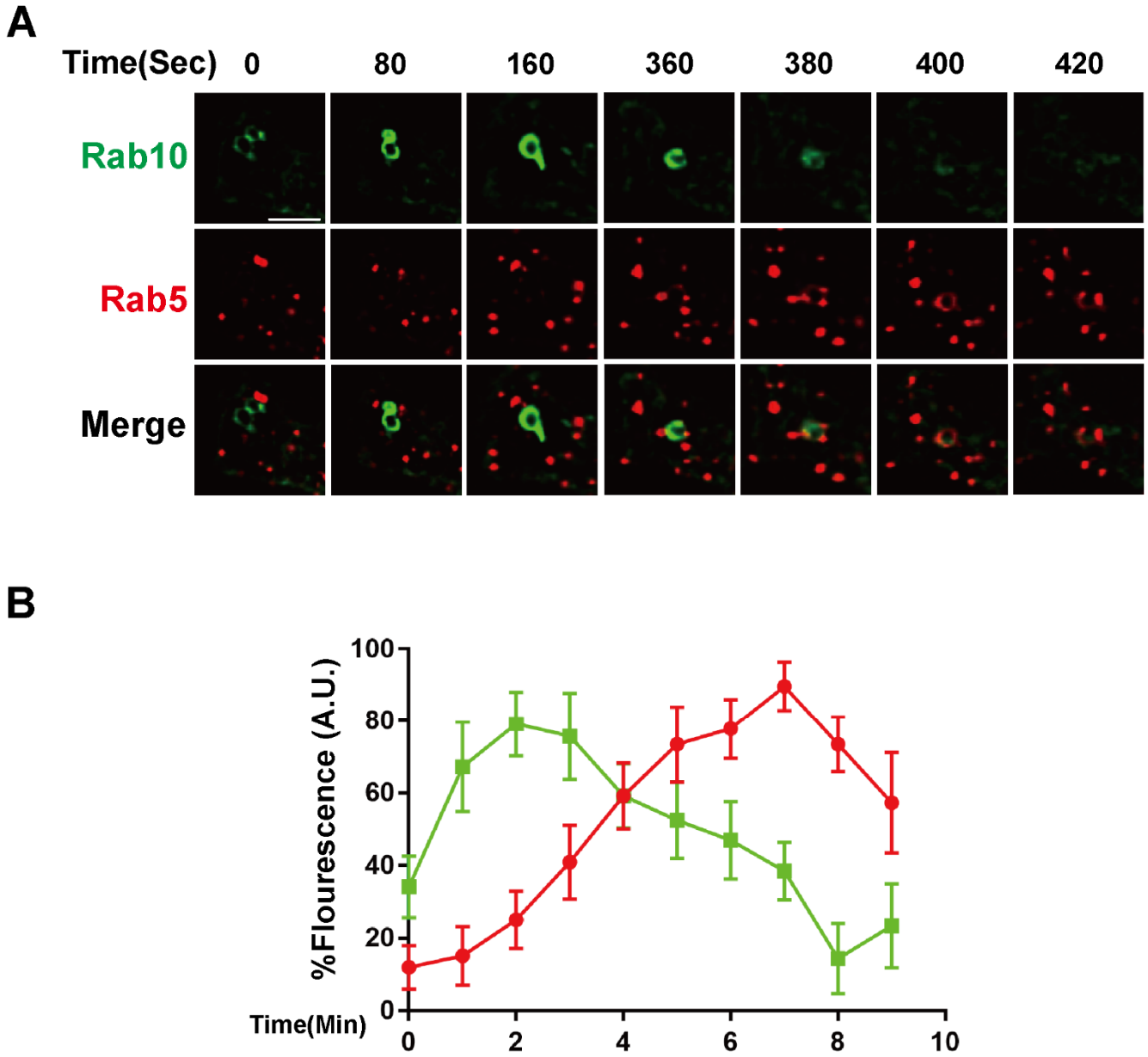

Extended data figure 4. Time-frame of Rab10 vesicles that become double-positive for Rab5

a, Raw 264.7 were co-transfected with eGFP(N-term)-Rab10 and mRuby(N-term)-Rab5 for 48 hours, with live-cell recordings for ~10 minutes. A representative vesicle is shown. Scale bar represents 1 μm. **b,** Calculated relative fluorescence over time is indicated from Rab10 positive vesicles, initially emergent from the plasma membrane, that become positive for Rab5. Data show >n=10 recorded vesicles across n=3 biologically independent experiments. Error bars show ± SEM.

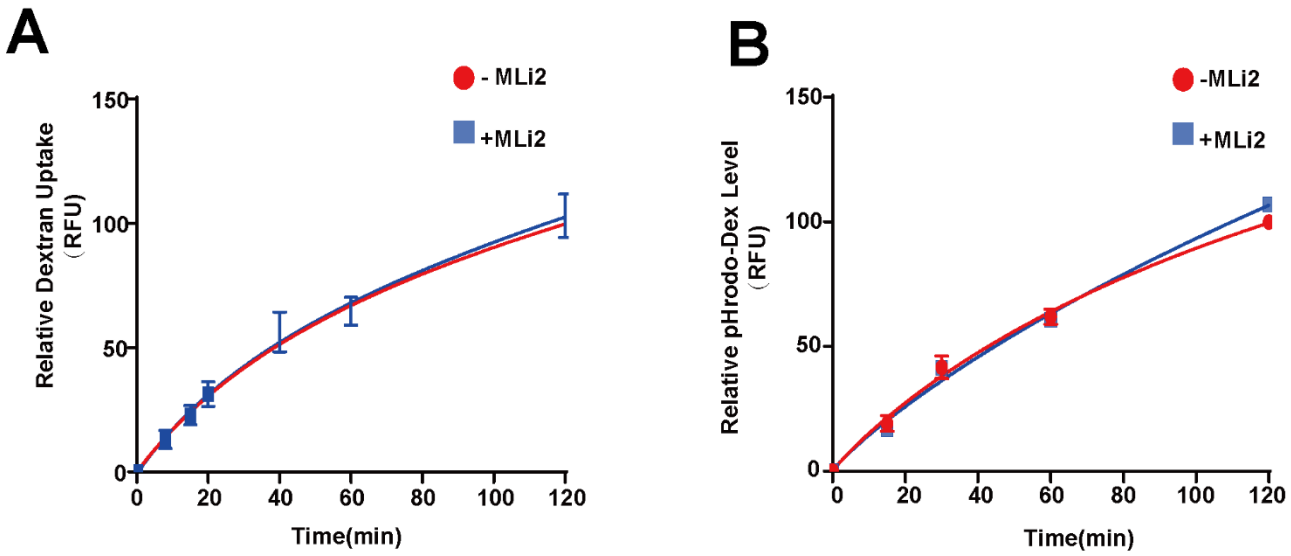

Extended data figure 5. Inhibition of LRRK2 kinase activity does not diminish macropinocytosis

a, Mouse bone marrow derived macrophages (mBMDM) were treated with DMSO or 100 nM MLi2 (LRRK2 kinase inhibitor) for 2 hours before incubated with TRITC-dextran or **b,** pH-Rodo-dextran for the indicated time points, followed by fixing, DAPI staining, and quantification of fluorescence. The relative fluorescence signal is calculated by subtracting the signal of cells incubated with dextran at 4 °C. Each data point is calculated from 15 images across n=3 biologically independent experiments, with error bars shown as ± SEM.

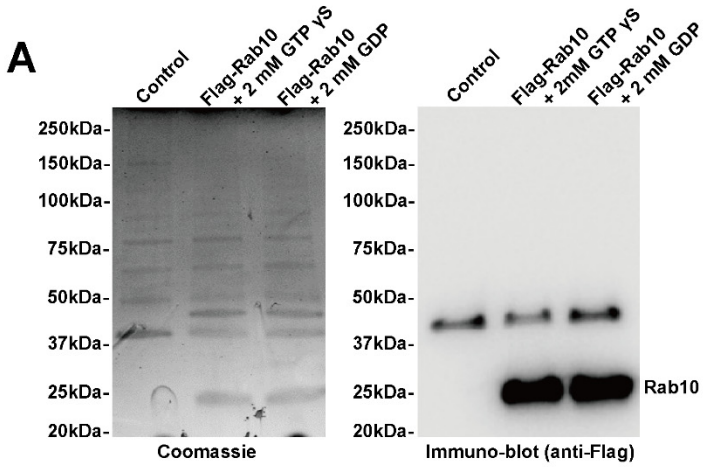

B

Protein	Rab10+GDP (Spectral Counts)	Rab10+GTP (Spectral Counts)	Control (Spectral Counts)
Rab10	1758	2064	4
Gdi2	1491	1762	5
Gdi1	362	398	0
Myo1e	66	0	0
Vps13c	29	34	5
Ehbp1l1	0	32	0
Myo5a	21	8	3
Ppp1r12a	17	7	2
Atp2a2	15	12	0
Myo1f	15	0	0
Mtmr14	13	3	0
Smarca2	11	0	0
Chml	8	10	0

Extended data figure 6. Identification of Rab10-interacting proteins in macrophage cells

a, Raw264.7 cells were transfected with Flag-Rab10 or control empty vector. The transfected cells were lysed in the presence of 2 mM GTPγS or 2 mM GDP. The Flag-Rab10 complex was immunoprecipitated with Flag-resin (sigma) followed by extensive washing and elution of complexes with 200 µg mL^{-1} 3xFlag-tide. (sigma). A portion of the eluted protein was analyzed by SDS-PAGE followed by Coomassie staining and immuno-blot with anti-Flag-HRP antibody. **b,** The eluted complexes were digested with trypsin and peptides identified with Orbitrap Mass Analyzer. A representative table of peptides matching proteins with spectral counts >10 from either the GTPγS or GDP incubations, and <10 spectral counts in the control elution.

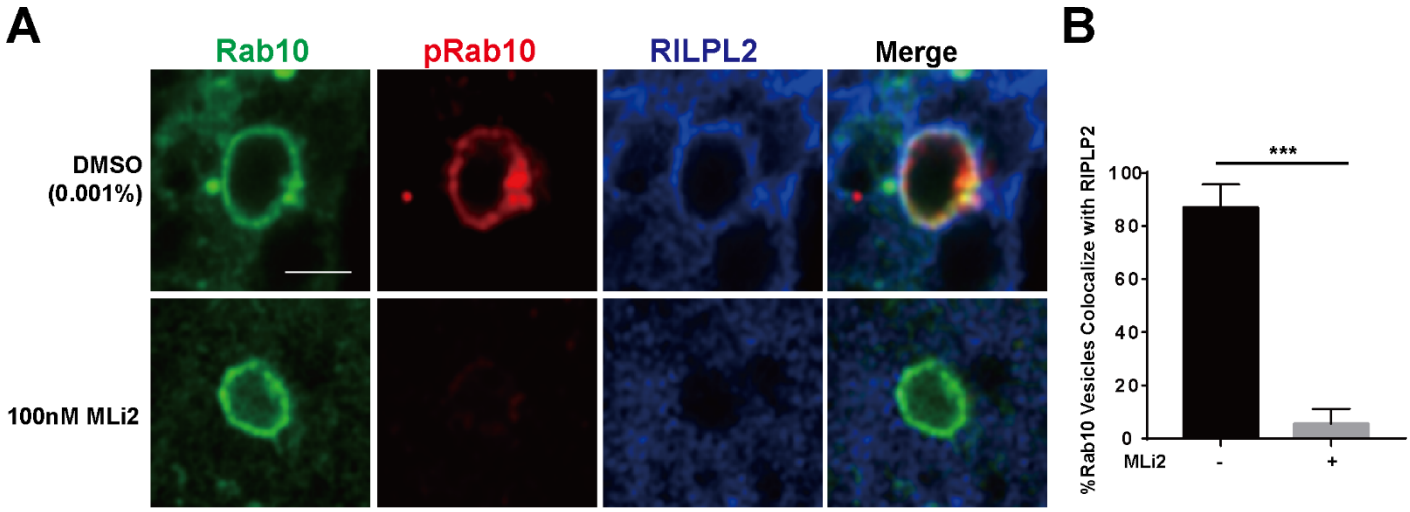

Extended data figure 7. LRRK2 kinase activity is required for RILPL2-binding to Rab10 vesicles

a, Raw 264.7 cells were co-transfected with eGFP(N-term)-Rab10 and Flag(C-term)-RILPL2. Cells were immuno-stained with anti-Flag antibody for RILPL2 (shown in blue), and anti-pThr73 for pRab10 (shown in red). Representative photomicrographs (from >30 images analyzed for each condition across n=3 biologically independent experiments) are shown. Scale bar represents 1 μm. **b,** Calculated percentage of GFP-Rab10 and Flag(C-term)-RILPL2 double-positive vesicles, with or without MLi2 treatment, were calculated from >30 images analyzed for each condition across n=3 biologically independent experiments. Error bars are shown as ± SEM and significance was assessed by one-way ANOVA with Tukey's post hoc test *$p < 0.01$.

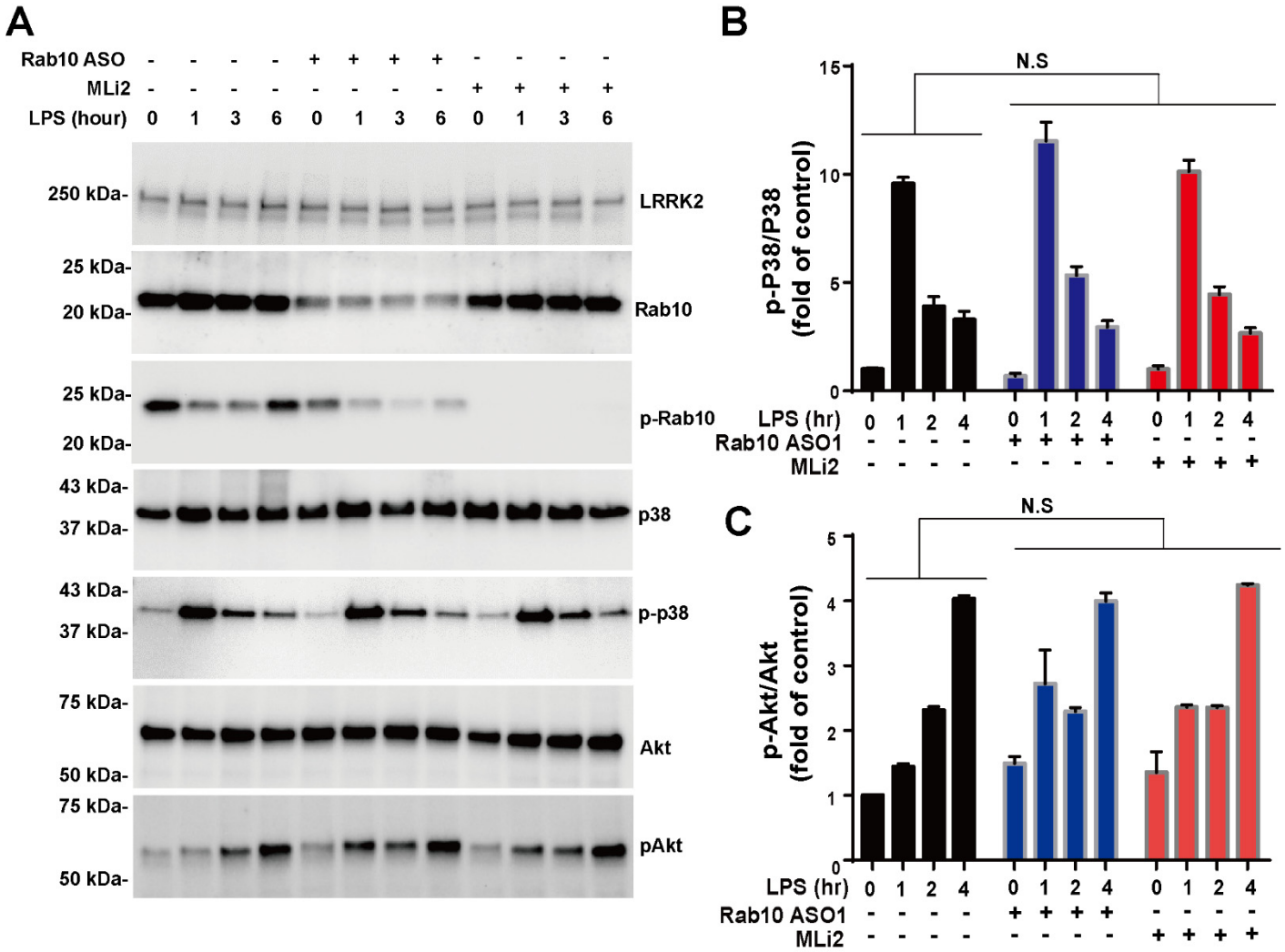

Extended data figure 8. Rab10 knockdown has no effect on TLR4-stimulated MAPK activation

a, Primary mouse bone marrow-derived macrophage cells (mBMDM) from adult male WT-mLRRK2 BAC mice were treated with DMSO, 1 μM Rab10 ASO for 4 days, or 100 nM MLi2 for 12 hours before stimulated with 100 ng mL^{-1} LPS for the indicated time points. Representative immune-blots from n=3 biologically independent experiments are shown. **b,** Relative Phospho-p38 MAPK (Thr180/Tyr182) levels were normalized to total p38 and calculated as the fold increase compared to control naïve (no LPS) cells. **c,** Relative phospho-AKT (Ser473) levels were normalized to total AKT and calculated as the fold increase compared to control naïve (no LPS) cells. Columns indicate mean values, with error bars showing ± SEM; significance for each group (0, 1, 2, or 4 hours post-LPS) was assessed by a two-way ANOVA, with n.s. indicating p>0.5.